CHARACTERISATION AND MODELLING OF THE SHEAR STRENGTH, STIFFNESS AND HYDRAULIC BEHAVIOUR OF ROCK JOINTS FOR ENGINEERING PURPOSES

Nick R Barton
Director, Nick Barton & Associates, Oslo, Norway

Stavros C Bandis †
Professor, Department of Civil Engineering, Aristotle University of Thessaloniki, GR
Principal, Geo-Design Consulting Engineers Ltd, UK

1 INTRODUCTION

The term 'characterisation' will be used to describe methods of collection and interpretation of the physical attributes of the joints and other discontinuities, in other words those which control their mechanical and hydraulic properties, and the behaviour of jointed rock as an engineering medium. Rock discontinuities vary widely in terms of their origin (joints, bedding, foliation, faults/shears, etc.) and associated physical characteristics. They can be very undulating, rough or extremely planar and smooth, tightly interlocked or open, filled with soft, soil-type inclusions or healed with hard materials. Therefore, when loaded in compression or shear, they exhibit large differences in the normal and shear deformability and strength, resulting in surface separation and therefore permeability. Such variability calls for innovative, objective and practical methods of joint characterisation for engineering purposes. The output must be quantitative and meaningful and the cost kept at reasonable levels. The practical methods to be described will be biased in the direction of quantifying the non-linear shear, deformation and permeability behaviour of joints, based on the Barton-Bandis (BB) rock engineering modelling concepts. The term 'modelling' will be used to introduce the basic stress-displacement-dilation behaviour of joints in shear, and the basic stress-closure behaviour when joints are compressed by increased normal stress. These are the basic elements of the (non-linear) behaviour, which are used when modelling the two- or three-dimensional behaviour of a jointed rock mass. They are the basic BB (Barton-Bandis) components of any UDEC-BB distinct element numerical model (used commercially and for research since 1985). The BB approach can also be used to determine improved MC (Mohr-Coulomb) strength components for a 3DEC-MC three-dimensional distinct element numerical model. In other words for acquiring input at the appropriate levels of effective stress, prior to BB introduction into 3DEC, believed to be a project underway. Due to space limitations, constant stiffness BB behaviour of rock joints is given elsewhere.

Keywords: joint characterization, roughness, wall-strength, peak strength, shear stiffness, normal stiffness, physical and hydraulic apertures (Quantification of parameters: JRC, JCS, φ_r, K_s, K_n, E and e)

2 BASIC GEOMETRIC INPUT FOR ROCK MASS REPRESENTATION IN MODELS

ISRM has recommended the following key attributes for the characterisation of rock discontinuities:

(a) Physical attributes affecting the engineering properties of discontinuities:

1) Roughness

2) Strength of rock at the discontinuity surfaces

3) Angles of basic and residual friction

4) Aperture of discontinuities

5) Infilling material

(b) Geometrical attributes defining the spatial configuration of discontinuities:

1) Joint orientations (dip & dip direction)

2) Spacing

3) Number of sets

4) Block shape and size

5) Joint continuity

In this chapter we will be addressing the characterization and quantification of the first 'smaller-scale' set (a) of *Physical attributes* in detail, and the effect each of them can have on the physical behaviour of the joints. We can use a photograph to introduce *(b) Geometrical Attributes* without going into further detail about these larger-scale structural-geology attributes of rock masses, which determine modelled geometries with UDEC-MC, UDEC-BB and 3DEC-MC. (MC Mohr-Coulomb, BB Barton-Bandis).

Figure 1 Characteristics of joint sets as observed in a Finnish open pit and at the portal of an old unsupported road tunnel in Norway (100 years prior to Q-system tunnel support guidance). We see variable orientation (dip and dip direction), variable spacing within each set, variable numbers of joint sets (two to three), variable block shape and size, and variable joint continuity (e.g. 1-10m and discontinuous).

In order to arrive at a credible final output, namely the mechanical properties of discontinuities, the 'characterisation' of the physical and geometrical attributes must adopt integrated approaches by combining *observations, measurements* and *judgment*.

Observations will cater for the intrinsic heterogeneity and variability and thus contribute to reducing 'sampling bias'. *Measurement* of the physical and geometrical attributes requires credible techniques that can be applied in the field and/ or in the laboratory in a standardised manner. Several techniques are available including index tests, laboratory tests and in situ tests. *Index tests* are simple, empirical methods, amenable to standardization and easily executable for measuring fundamental 'indices', such as friction, rock strength, roughness, etc. *Laboratory tests* (e.g. direct shear, uniaxial compression) are useful for confirmation of engineering properties predicted by index testing, notably when special types of discontinuities are involved (e.g. infilled or intensely pre-sheared). *In situ tests* may also be used for deriving parameters at representative geometrical scales and to study behavioural trends of particular critical discontinuity types, such as major weak features (e.g. fault zone materials).

Geometrical and other factors such as continuity, block size, history of displacements, etc. need to be taken into account when interpreting the characterisation data in order to derive engineering properties. It is at that stage of characterisation that expert *engineering judgment* acquires a special role.

3 CHARACTERIZATION AND QUANTIFICATION OF JOINT PROPERTIES

A convenient assembly of the recommended index tests needed for applying the Barton-Bandis BB model is shown in Figure 2. These tests, including the direct shear tests, were used by Barton and Choubey, 1977 in their comprehensive research and developments using 130 joint samples collected from road cuttings near Oslo, Norway. The sketches were developed in the form of coloured 'over-heads' for lecture courses, and bought together in one figure in Barton, 1999.

Fortunately for the more rapid development of the BB model, Bandis, 1980 used the same methods for characterization and description of his numerous joint replicas (used in his scale-effect studies) and for his natural joint samples (used for his normal stiffness studies). The suggested parameters from Barton, 1973: JRC, JCS and ϕ_b were expanded to include the potentially lower ϕ_r for weathered joints because of the sometimes slightly weathered joints tested by Barton and Choubey, 1977. Following Bandis, 1980 Ph.D. studies, the combined techniques for modelling both shear and normal loading were published in Bandis et al. 1981 (mostly concerning shear behavior and scale effects) and in Bandis et al. 1983 (most concerning normal stiffness behavior). In Figure 2 histograms can be seen for (suggested) presentation of variability within each index test. For example JRC is given with subscripts JRC_0 and JRC_n. These represent nominal 100mm long or larger-scale values, which might be obtained by the a/L method of Barton, 1981. This is also shown in Figure 2, and expanded upon later in this chapter.

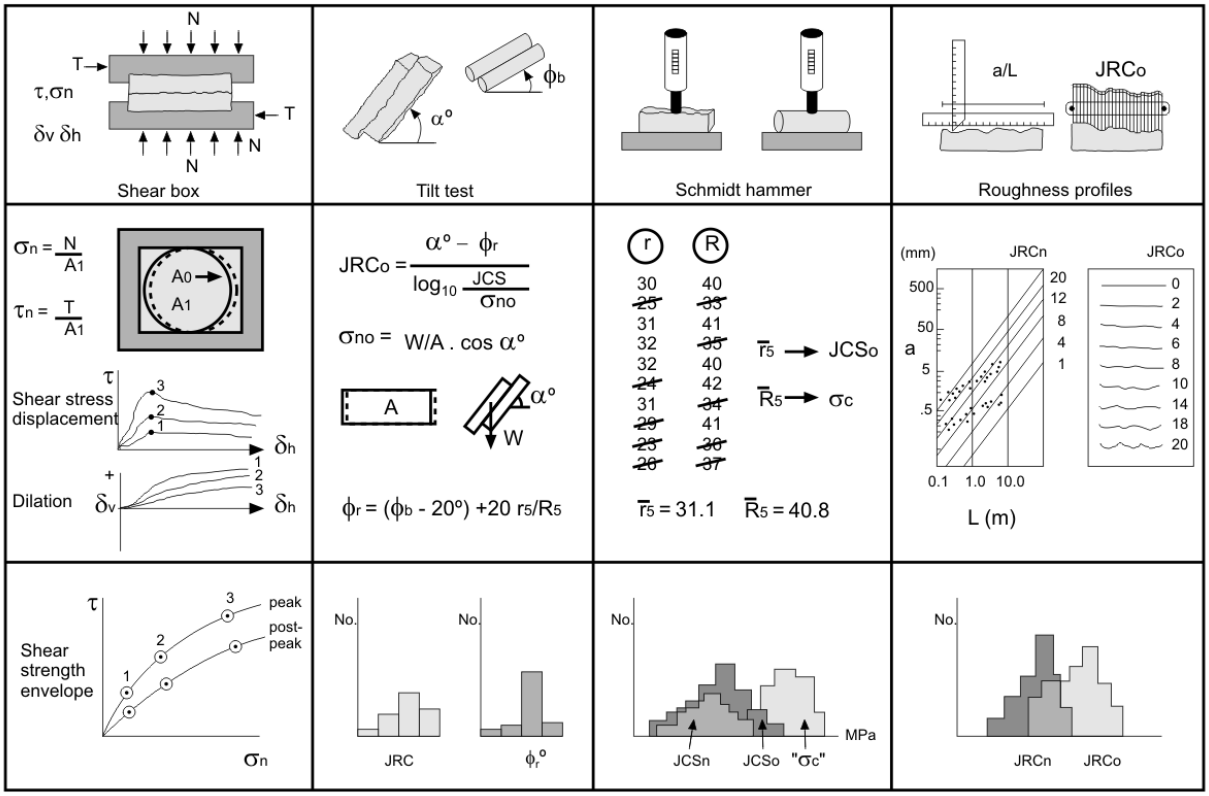

Figure 2 Four columns of diagrams showing 1. direct shear tests principles (Note: apply shear force T 'in-line' to avoid creating a moment), 2. tilt test principles, 3. Schmidt hammer test principles, and 4. roughness recording principles. Each of these simple methods are described in the following paragraphs.

Since direct shear tests may be performed as part of the site characterization studies, some short notes are provided, which may or may not perfectly conform with suggested methods. However they are the result of collectively performing many hundreds of direct shear tests on rock joints, rock joint replicas, or rougher tension fractures.

1. *Direct shear tests:* The joint samples may consist of (cored) nearly circular or elliptical, or (sawn) square or rectangular samples, i.e. prepared from core, or from sawn blocks recovered from adits or from freshly excavated rock slopes. A strong recommendation is to recover sufficient numbers of representative samples of each joint set of interest, so that multiple testing of the same sample is avoided. The latter tends to 'rotate' the shear strength envelope, when tests at low stress are succeeded by tests at higher stress. An (even more) artificial 'cohesion' intercept is thereby obtained. (See discussion in Barton, 2014). Shear stress-displacement curves and dilation-displacement curves are plotted, and may look similar to the sketches in panel 1.2. The third Panel 1.3 shows 'peak' and ultimate' strength envelopes which will tend to be curved if joints have significant roughness and/or if a significant range of normal stress is applied, such as 0.5 to 5 MPa, or 1 to 10 MPa. Note that residual strength envelopes are highly unlikely to be reached with just a few millimeters of joint shearing (≈ 1% x L may be needed to reach peak, or

1mm in the case of a 100mm long sample. This 1% reduces when testing longer samples). A method of estimating an approximate residual strength based on Schmidt-hammer tests is shown in Figure 2 (combine Panel 3.2 with Panel 2.2). It will be found that $\phi_r < \phi_b$, usually by several degrees if joint weathering (r < R) is significant.

2. *Tilt tests:* It is believed that Barton and Choubey, 1977 were the first to apply tilt tests in a 'scientific' way to determine specific 'designer-friendly' joint strength properties, since they showed how both ϕ_b and JRC could be obtained from tilt tests. Because a sound empirical non-linear shear strength criterion is used (Panel 2.2), the tilt test result from gravity shear-and-normal loading at a failure stress as low as 0,001MPa can be extrapolated by three to four orders of magnitude higher normal stress. We will of course reproduce the 'standard set' of 100mm JRC profiles very soon, but in the meantime emphasize that many who concentrate (in the last decades) on the exclusive use of 3D-laser profiling of roughness, may be missing some important details of shear behavior by never performing (3D) tilt tests and 'always' criticizing 2D roughness profiles. (The latter were always intended just as a rough guide, and some 400 could have been selected to represent the typical (direct shear tested) JRC values of Barton and Choubey, 1977, since 3 x 130 tilt tests were performed and 3 x 130 2D profiles were recorded. (The representative JRC values were however selected from among the single DST tests on the same130 joint samples). Panel 2.1 represents the tilt test principle for testing the natural joints for back-calculating JRC, shown in Panel 2.2. Panel 2.1 also shows tilt tests on core sticks (these could be sawn blocks). The way in which the basic friction angle ϕ_b is utilized is shown in Panel 2.2. In the case of using artificially 'prepared' surfaces for ϕ_b it is important to avoid using 'polished' samples due to slow drilling or slow diamond sawing. Brief sand-blasting should be performed to expose the mineralogy, without adding roughness. If ridges are present across either type of sample then grinding away of the ridges followed by sand-blasting should be sufficient. Values of ϕ_b tend mostly to be in the range 25° to 35°, and most frequently 28° to 32°. However if a single rock type like chalk or limestone is of interest, values may be consistently close to the upper values. Please be aware that 'so-called ϕ_b values' obtained by subtracting dilation angles from peak shear strength may be (dangerously) over-estimated, due to neglect of the asperity failure component a_s (which is of similar magnitude to the dilation angle). This will be illustrated later.

3. *Schmidt-hammer tests (for JCS).* Panel 3.1 illustrates, in diagrammatic format, the use of Schmidt-hammer rebounds (respectively r or R) when measuring on natural joint surfaces, and when measuring on artificially 'prepared' surfaces (core-sticks or sawn blocks). In each case, a flat concrete laboratory floor and clamping to a steel 'V-block' base is advised, so that the impact and

rebound are not affected by unwanted 'rocking' or other movements. However, to be on the safe side and in order not to have the effect of crushing a loose mineral grain, the mean of the top 50% of measurements is found to be superior to the normally recommended mean values. This simple technique is shown in Panel 3.2. Artificially low vales are thereby removed as unwanted 'noise', and the remaining 50% tend to be more uniform and therefore more representative. So finally, the mean values of r_{50} and R_{50} are used to represent, respectively, the ***JCS (joint wall compressive strength)*** and an approximate measure of UCS (unconfined compression strength). Of course more direct measurement of the latter are usually a part of the site investigation.

4. *Roughness measurement (for JRC).* Panel 4.1 of Figure 2 illustrates the two principal methods for recording joint roughness, and estimating JRC. Panel 4.2 shows in symbolic format, the a/L method and the JRC-profile matching method. A nearly full-scale set of roughness profiles of characteristic 100mm length, with associated JRC_0 estimates, from nearly smooth-planar JRC = 0 to 2, up to extremely rough, undulating JRC = 18 to 20, are reproduced on the next page for ready reference. However tilt testing where possible, or amplitude/length (= a/L) measurements are recommended, in addition to profile 'matching', because the latter is inevitably subjective. This was pointed out not only by the first authors, but probably by each of the researchers responsible for a reported 49 equations for JRC (seen tabulated in a 2016 paper review). None were interested in performing tilt tests it seems. Figure 3 reproduces the original roughness profile from Barton and Choubey, 1977.

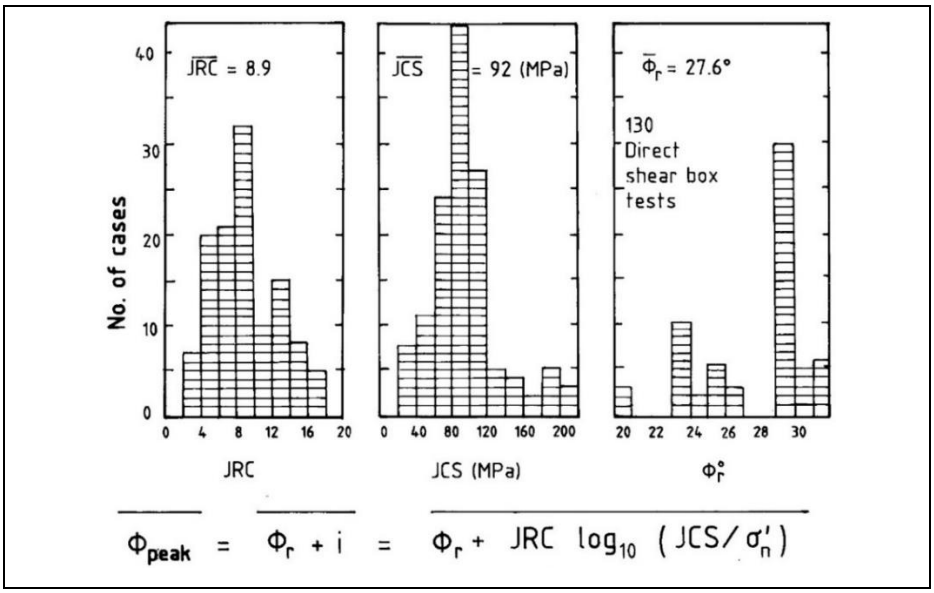

Figure 3 The results of characterization of JRC and JCS and testing (tilt test and DST) one hundred and thirty rock joint samples. Note that the 'i-value' of Patton, 1966 is replaced by a stress-dependent logarithmic function incorporating variable (and scale-dependent) roughness, and the ratio of normal stress and joint wall strength, the latter also scale-dependent. The strength envelope is non-linear.

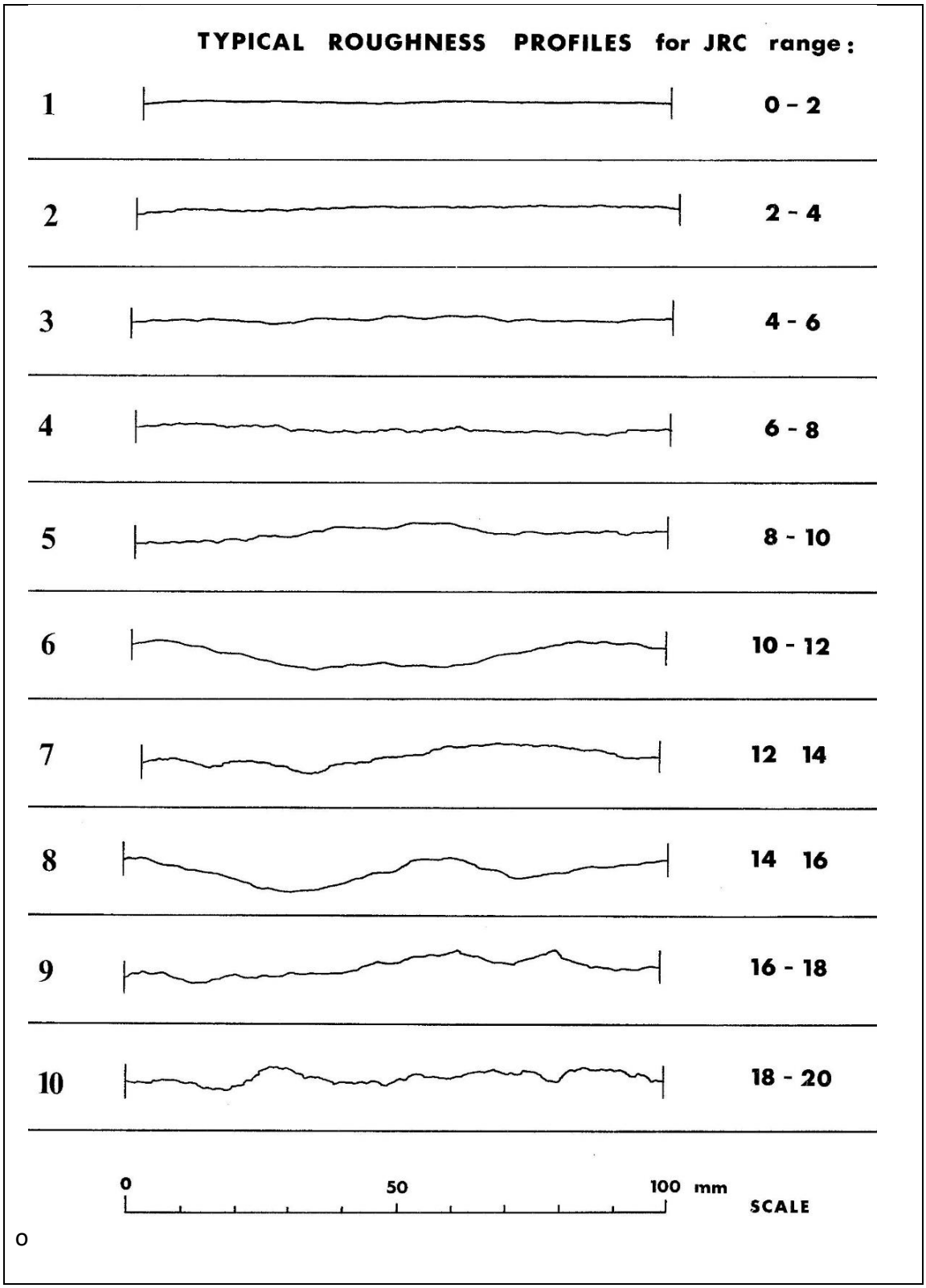

Figure 4 The 100mm long roughness profiles were associated in each case with back-calculated JRC values in the given range, based on direct shear tests of the individual joint samples. In each case, three roughness profiles were recorded on each sample, and one was chosen as representative. In each case, three tilt tests were performed on each sample, so as to predict the DST. Barton and Choubey, 1977.

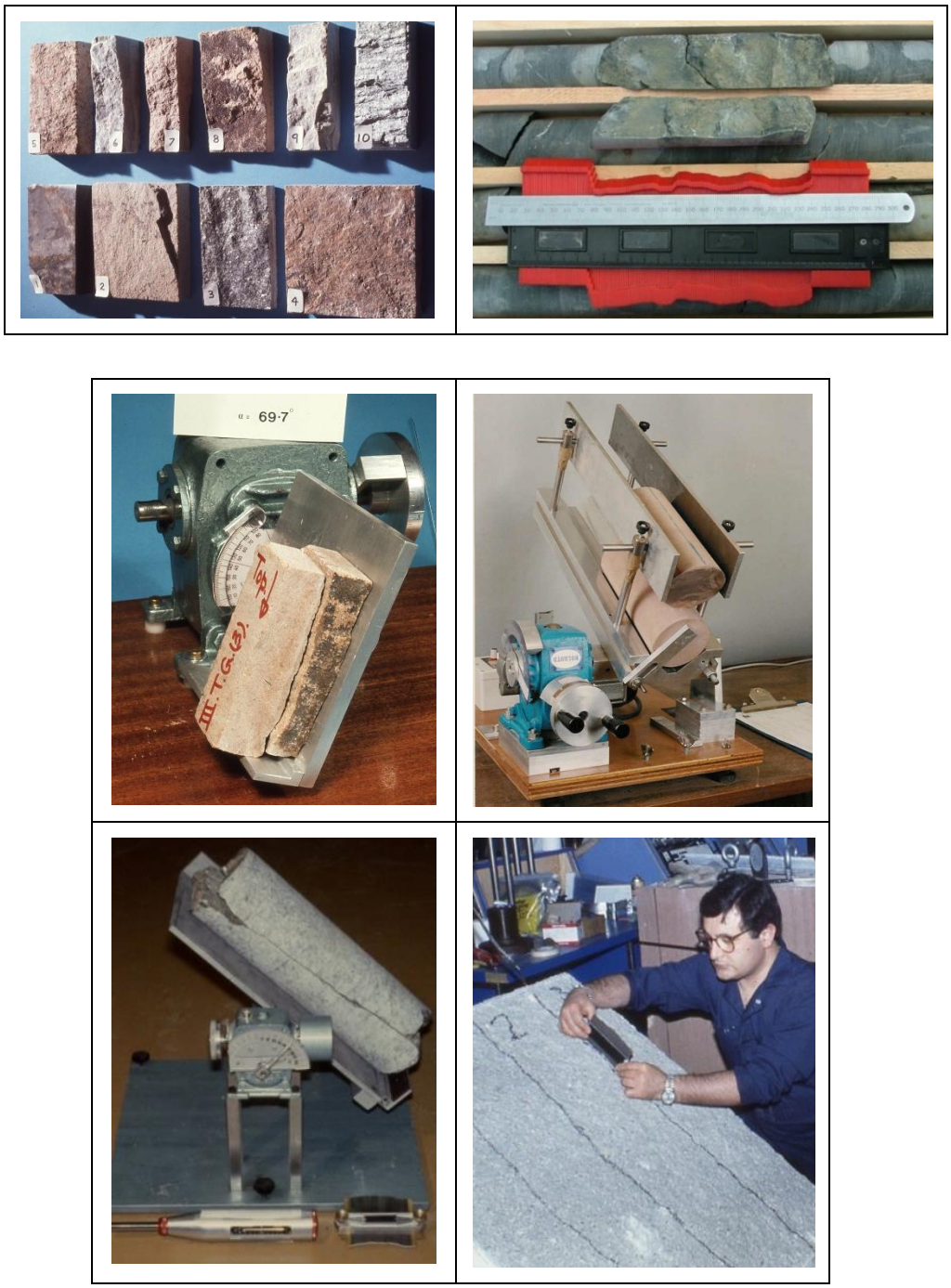

Figure 5 From top-left: a) The ten joint samples profiled in Figure 3. b) During core-logging (for Q-parameters) JRC is estimated using the profilometer and the a/L method (note magnets holding steel rule). c) One of the tilt-tests performed by Barton and Choubey, 1977. d) An electric-motor driven tilt test of φ_b using core-sticks (no ridges, no polish). e) Tilt test on large core showing Schmidt hammer and roughness-profiling comb. f) Roughness recording at 150mm and 1300mm scales, on fractured 1m^3 blocks, prior to 1.3 ton tilt-tests, followed by biaxial flat-jack shear test (Bakhtar and Barton, 1984).

A practical and economic design for a tilt-test apparatus is shown in Figure 6. This was developed while the first author worked in TerraTek, with various joint characterization and testing projects. Today the company is owned by Schlumberger, and one may guess that this petroleum service

company is less oriented for fracture characterization of reservoir rocks due to scarcer sources of samples, and the unfortunate tendency (from a rock mechanics point of view) of sectioning core, thereby losing the possibility of testing circular or elliptical samples. Furthermore, there is the remarkable tendency of those practicing reservoir geomechanics of only using linear friction coefficients (from Byerlee, 1978) and linear Mohr-Coulomb strength envelopes for the matrix rock. Both methods have severe limitations in terms of interpreting reservoir behavior because effective stresses rise by tens of MPa with increased production.

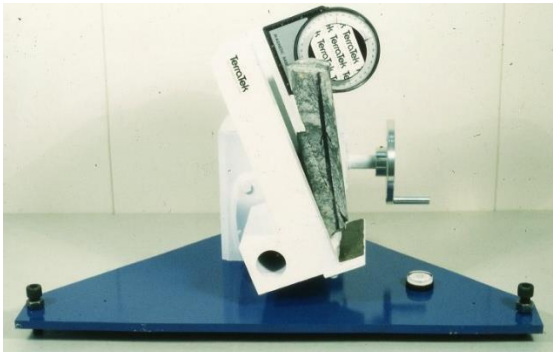

Figure 6 An economic tilt test apparatus, which consists of a triangular steel base-plate with three levelling screws, a circular spirit level, a tilt-angle recorder, a heavy 1:200 reduction gear (with rotating handle), and a core-shaped or V-notch shaped 'tilt-table' which must be screwed to the gear axle at one end, so that the turning moment remains anti-clockwise (when viewed from front) throughout the tilt test. (One must avoid vibration occurring due to 'gear-slack' just before sliding occurs, as then the correct tilt angle will be missed).

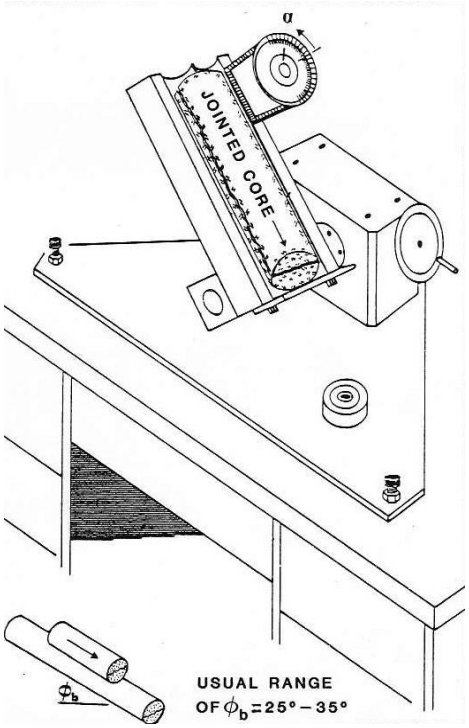

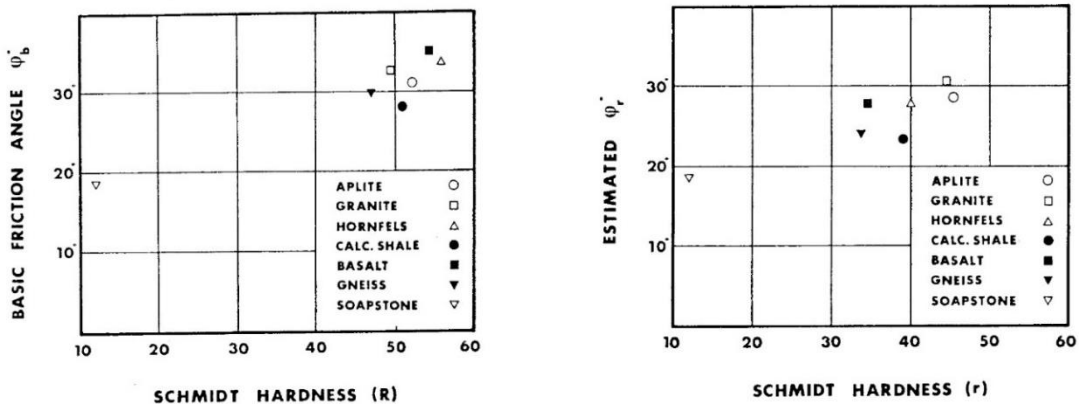

Figure 7 The Schmidt L-hammer is a useful way to register the degree of weathering in a rock joint. This method was used long ago by Richards, 1975 for registering the weathering grades (and low residual friction angles) of joints in sandstones, where values as low as φ_r = 12° and r as low as 15 were recorded.

Figure 7 illustrates the way that the residual friction angle (ϕ_r) correlates approximately with the Schmidt hammer rebound (r). It is estimated from the empirical equation shown in Figure 2 (bottom of Panel 2.2) The reduction from (R) to (r) due to weathering effects was illustrated in Figure 2 (Panel 3.2). As a result of the three components JRC, JCS and ϕ_r we see the non-linearity sketched in Figure 8, in contrast to Mohr Coulomb linearity, or Patton, 1966 bi-linearity.

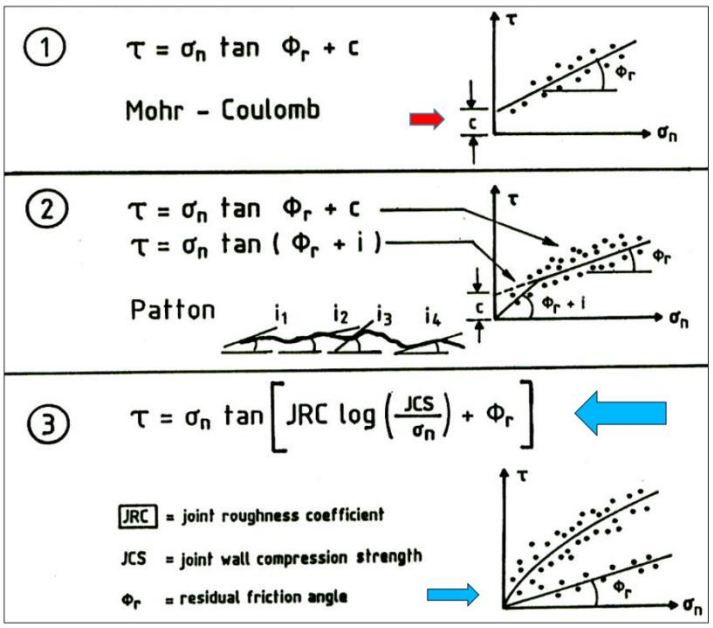

Figure 8 Diagrams and equations representing the most common shear strength criteria for rock joints: Mohr-Coulomb, Patton, 1966 and Barton and Choubey, 1977.

When block-size is taken into account, and we move beyond nominal laboratory L_0 = 100mm samples (where JRC_0 and JCS_0 apply), then input data applies to block-size L_n (the mean cross-joint spacing of each set) and we will refer to JRC_n and JCS_n . It is then correct to refer to the Barton-Bandis criterion, as scale effects are accounted for following the block-size scale effect adjustments suggested by Bandis et al. 1981. Note the red arrow in Figure 8, next to the actually non-existing cohesion (c) which is an artifact of the M-C linearity assumed. Only joints with steep steps, such as cross-joints, have real cohesion. When testing at very low normal stress (see small blue arrow) the friction angle may become very large, and the 'limit' is the tilt test, commonly performed at 1000 to 10,000 times lower stress than in rock engineering designs. Since envelope curvature is correct, a good estimate of engineering performance is achieved, as verified in Barton and Choubey, 1977 who studied and proved the validity of the normal stress 'jump' from 0.001 MPa to 1 MPa (approx.) This is also discussed in Barton, 1999, where the important topic of stress transformation errors is introduced: as applying to 45° loaded-direction shear test apparatuses.

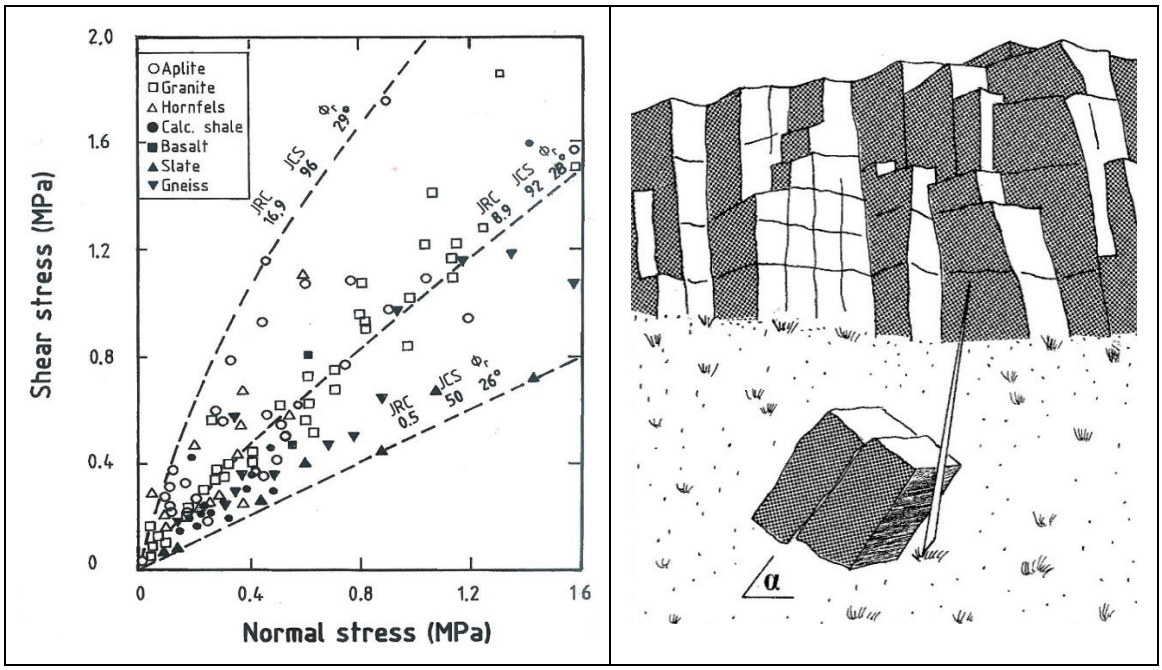

Figure 9 The DST measured peak shear strengths of the 130 joint samples, whose JRC, JCS and φ_r statistics were summarized in Figure 3. The symbolic tilt-test block is designed to emphasize that the shear strength of rock joints can be estimated from index tests carried out on recovered core or blocks of rock, if the latter are freshly exposed in e.g. rock cuttings or open-pit benches. 3D laser and long equations are not needed.

The direct shear test results for joints recovered from the seven different rock types are shown in Figure 9. Deliberate choice of highest and lowest JRC, JCS and ϕ_r values allow the curved upper-most envelope and the lowest, almost linear envelope to be drawn. In the latter JRC is only 0.5 ('smooth, planar') compared to JRC = 16.9 ('rough, undulating') for the upper envelope. The mean results of the three parameters (JRC = 8.9, JCS = 92 MPa and ϕ_r = 28°, are shown by the central envelope.

Regrettably in *geomechanics for petroleum,* there is an almost universal tendency (oil companies on both sides of the Atlantic and in the Middle East) to use the so-called 'Byerlee law', in which a (linear) friction coefficient of 0.85 (ϕ = 40.4°) is assumed to represent 'critically stressed' fracture sets or joint sets. Byerlee was clearly not happy with three joint parameters (JRC, JCS etc), and generations of (Stanford) researchers and professors have followed his simple (and sometimes very inaccurate) linear and limited friction coefficient approach. The need for more accuracy and acknowledgement of the actual important role of rock type and roughness are nicely emphasized by the following classic µDEC (pre-UDEC) result from Peter Cundall and a former Ph.D. student Mike Voegele. Only the most stable case shown in Figure 10 corresponds to the Byerlee 'law'. The linear 'belief' has been further spread by Zoback, 2007. Cross-Atlantic research (on non-linear description for rock joints) does not seem to be popular in geomechanics, despite 65% of remaining petroleum in naturally fractured reservoirs (NFR) with guaranteed non-linear behavior. See Barton, 2015 and Barton, 2016 for further discussion.

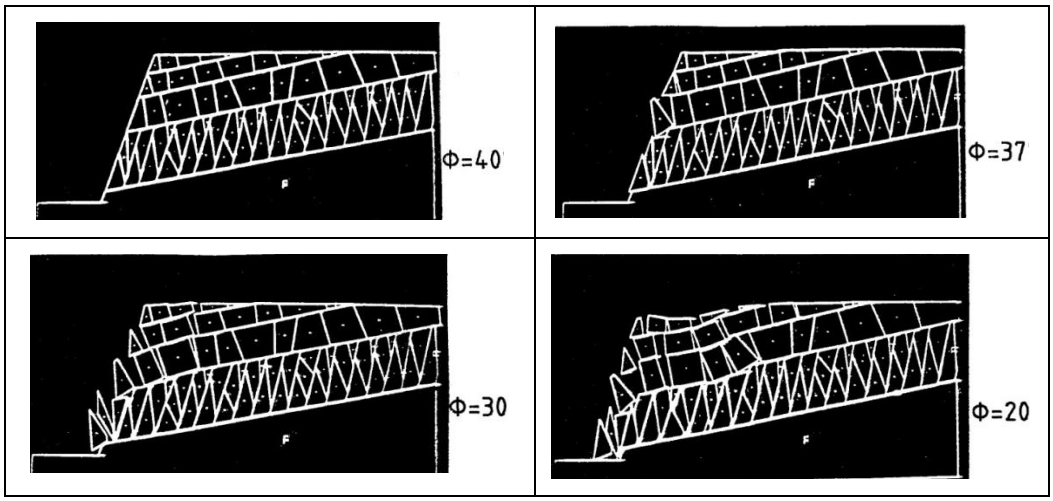

Figure 10 The importance of variable frictional angles on rock slope stability (and indeed on slope deformation characteristics) are nicely illustrated by these early distinct element (µDEC) models which was a method developed by Cundall, and culminated in UDEC (UDEC-MC and UDEC-BB) and 3DEC-MC. These four slope models are from Cundall et al. 1977. The given friction angles applied to all joints in these cases. Today we can model deformable blocks (in UDEC) and differentiate the (possible) non-linear response of the different joint sets (the latter with UDEC-BB, commercially available since 1985).

4 QUANTIFICATION OF JOINT PROPERTIES AT LARGER SCALE

There have been various stages in the profession's acknowledgement of the need for scale-effect adjustment concerning the shear strength of rock joints. In particular, the studies at different scales by Pratt et al. 1977 (using in situ tests), by Barton and Choubey, 1977 (see Figure 11), by Barton and Hansteen, 1979 (using studies with different block sizes in 250, 1,000 and 4,000 tension-fracture block-assemblies) and especially by Bandis, 1980 and Bandis et al. 1981 (from work with different size replicas of rock joints), leaves one in no doubt about the importance of scale effects. We will also see tilt test results and roughness profiling in relation to typical large-scale JRC_n values, from 130 cm long fractures tested by Bakhtar and Barton, 1984. JRC_n is lower than JRC_0, and as we shall see, this has a significant effect on shear strength-displacement behaviour.

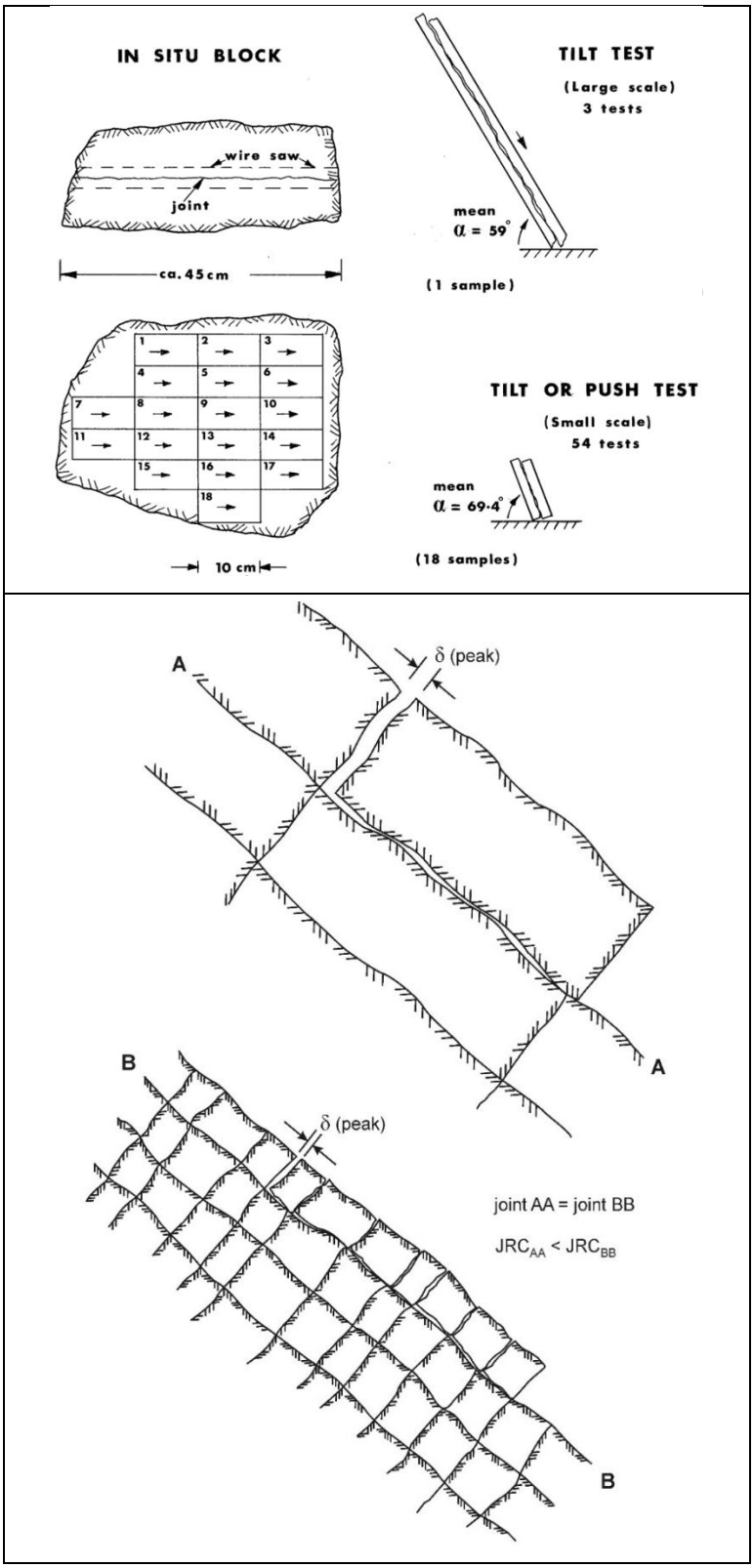

Figure 11 Scale-effect investigation with tilt-tests of a 45 cm long joint in granite, followed by individual tilt tests on eighteen component samples from the same joint, sheared in the same direction. The JRC value increased from 5.2 to 8.8, and eight of the eighteen samples now had to be push-tested as 'so rough'. Shear strength is lower for the largest sample, and the displacement to reach peak (δ_{peak}) is also larger.

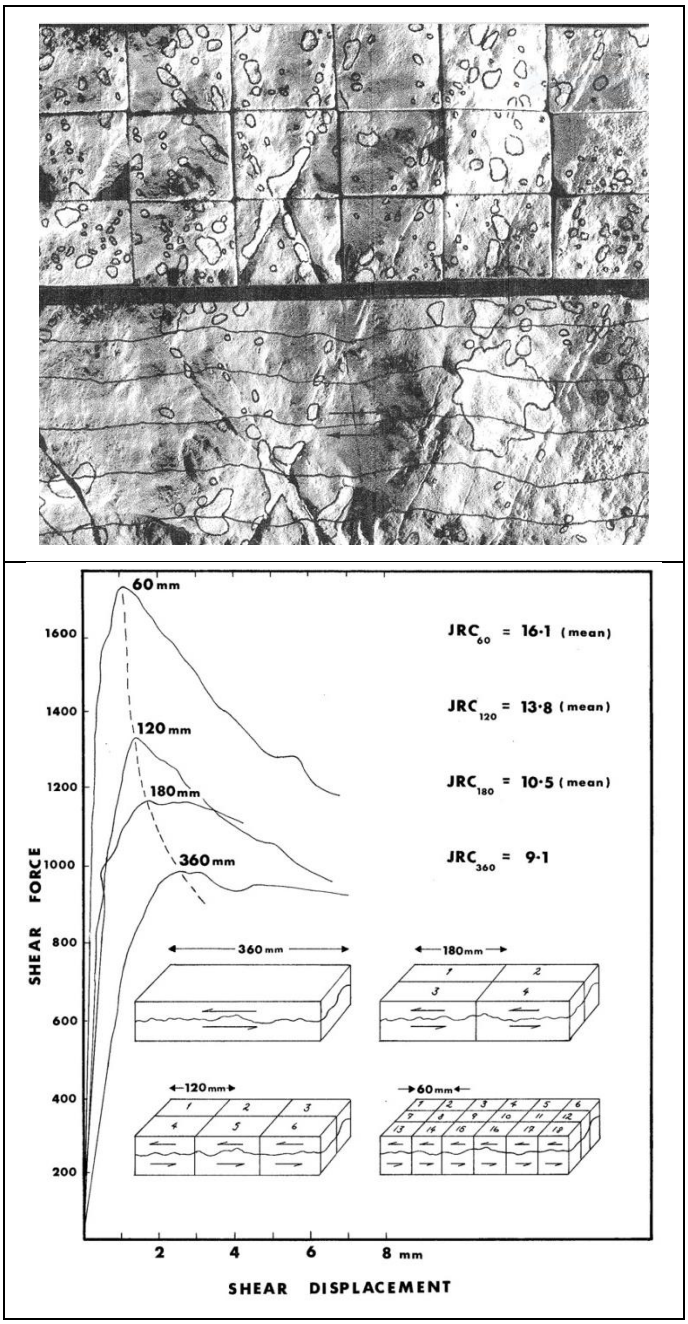

Figure 12 Some of the scale-effect studies of Bandis, 1980 which were journal-reported in Bandis et al. 1981. Replicas of natural rock joints could be reproduced many times, and therefore could be tested at different scales. This particular set shows some specific changes in contact areas, reduced JRC and increased δ_{peak}.

The joint replica tests performed by Bandis, 1980, and parallel sets of normal-closure tests on natural rock joints (see later) were each described by the JRC, JCS and ϕ_r parameters developed in Norway in the preceding years. An important summary of the scale-effects observed by Bandis is given in Figure 13. Here we see use of the asperity failure components S_A of Barton, 1971, which may be of the same (angular) magnitude as the peak dilation angle. It is not correct to assume that this component is zero, and by subtracting the dilation from peak strength to assume one has reached 'basic' (flat surface) friction angle.

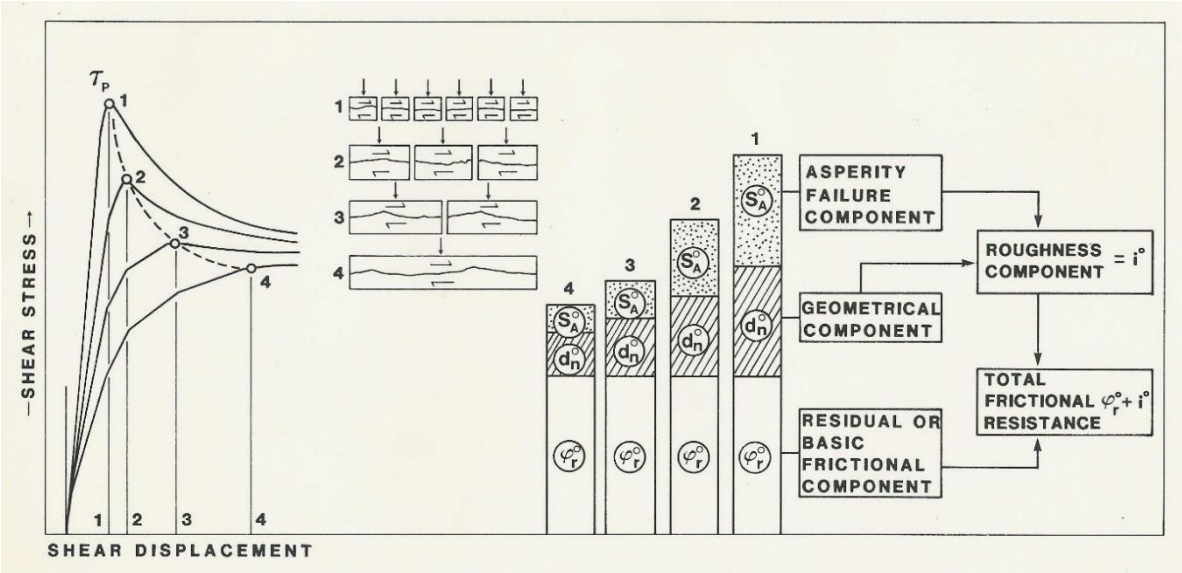

Figure 13 The principal scale-dependent components of the shear strength of rock joints as summarized by Bandis, 1980 and Bandis et al.1981. Note that S_A has almost the same magnitude as the peak dilation angle, at various scales, so subtracting dilation from peak strength leaves two components remaining, not φ_b as assumed by Hencher on various occasions.

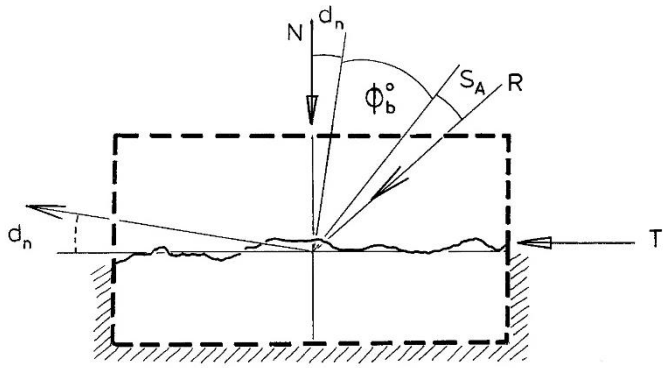

Figure 14 The angular components of shear strength for a non-planar rock joint. Barton, 1971. Note that the presence and influence of dilation d_n requires adjustment of the classic stress-transformation equations for all shearing-and-dilating geotechnical materials. (See Bakhtar and Barton, 1984 and Barton, 2006). This important topic will be discussed later in this chapter.

The scale effects illustrated in Figure 13 are the 'product' of individual scale effects on JRC and JCS, and as a result of combining the results of Barton and Choubey, 1977, Barton and Hansteen, 1979 and Bandis 1980, the following suggestions for reductions of JRC and JCS with increasing block size were given by Bandis et al. 1981. The following equations were recommended:

$$JRC_n \approx JRC_o \, [\, L_n/L_o \,]^{-0.02\, JRC_o} \qquad (4)$$

$$JCS_n \approx JCS_o \, [\, L_n/L_o \,]^{-0.03\, JRC_o} \qquad (5)$$

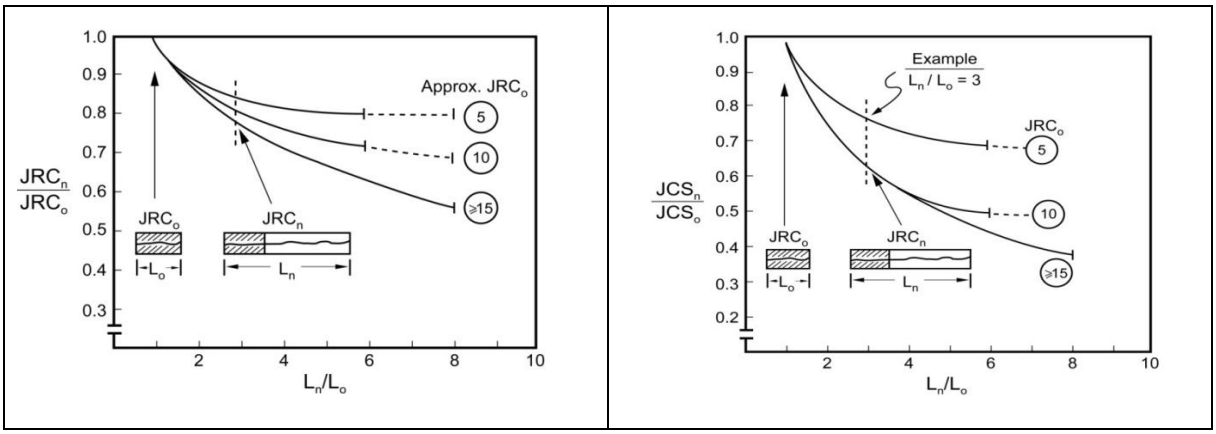

Figure 15 When representing the shear strength of rock masses with the parameters JRC and JCS, it is necessary to consider the mean spacing of joints crossing the joint set of primary interest, in order to apply the scaling equations 4 and 5 of relevance to this block size (say 2 m). The spacing of joints crossing the joint set of secondary interest (say 3m) will define the mean block size for the secondary set.

The tests shown in Figures 16 and 17 were performed by Barton on tension-fractured brittle model materials, using a double-bladed guillotine for generating intersecting sets of equally-spaced fractures. The tests (which were pre-UDEC, and therefore pre-UDEC-BB) were performed prior to large-span cavern modelling (for underground *nuclear power plant* purposes), using various fracture configurations and stress levels. Although the deformation moduli of the smallest-block models were lowest, the greater freedom for block rotation in these cases gave them higher shear strength, and induced kink-band formation.

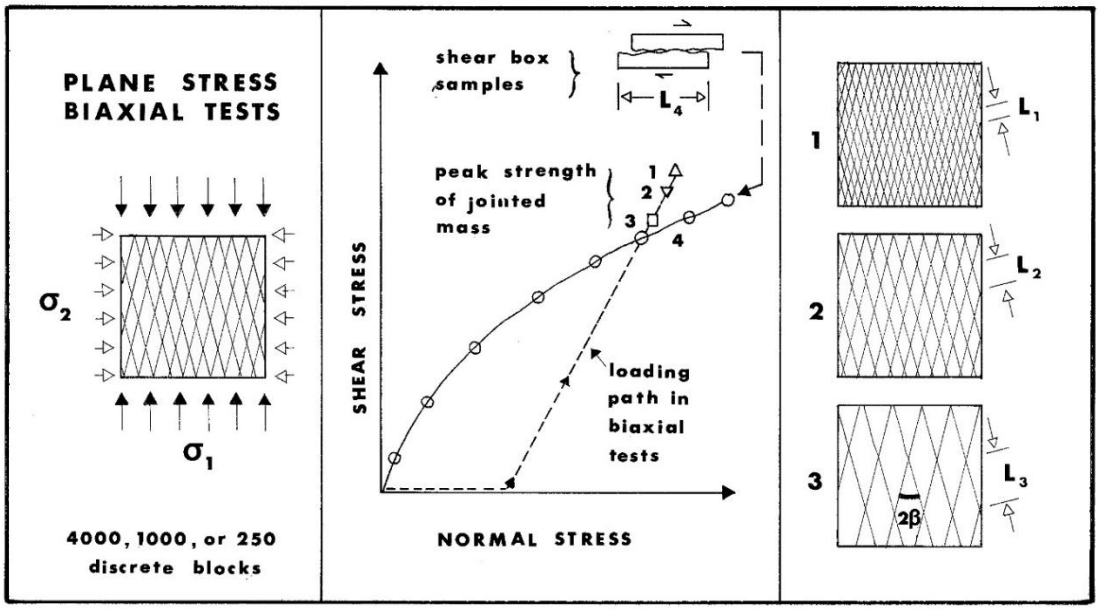

Figure 16 Biaxial shear strength testing of (guillotine-tension) fractured block assemblies consisting of 250, 1,000 and 4,000 distinct blocks. The first set of parallel fractures were continuous, while the second set crossing the first had potential cohesion, due to the steep steps created. Barton and Hansteen, 1979.

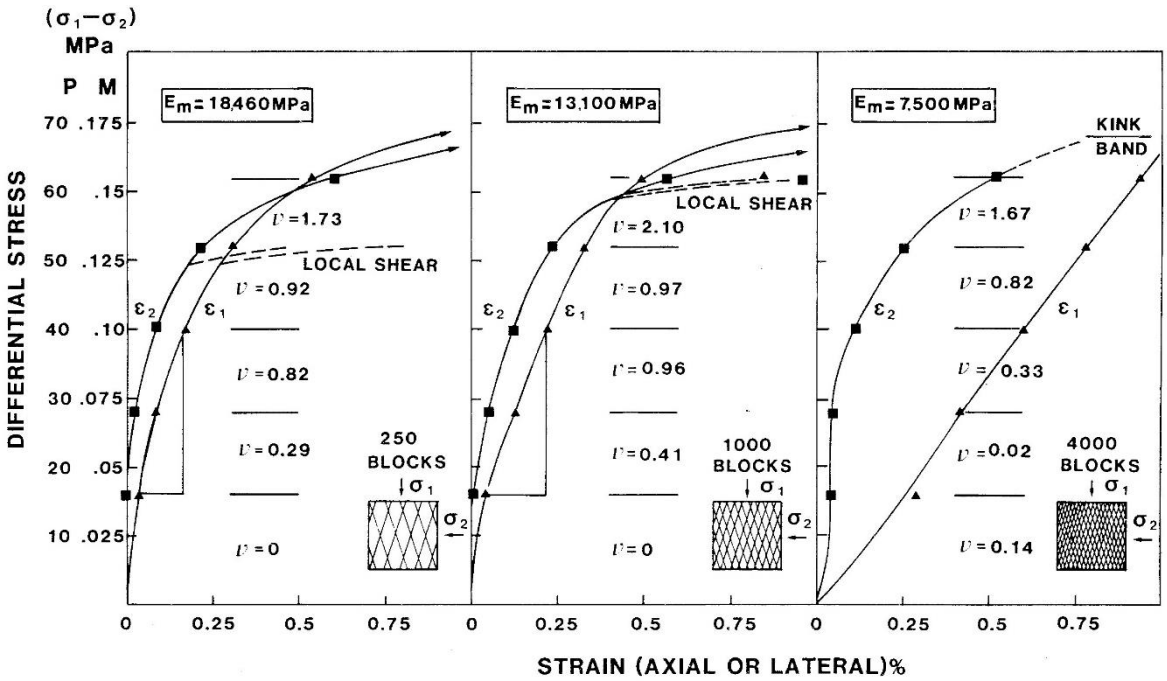

Figure 17 The reductions in block size shown symbolically here, had a consistent tendency to cause higher shear strength. However, in the case of the smallest blocks, whether with 60°/60° or 45°/45° fracture orientation, there was a remarkable 'linearization' of the stress-strain diagrams. Note the strong increases in the 'lateral expansion coefficient' (jointed Poisson's ratio) due to joint shearing (and violation of continuum behavior). Barton and Hansteen, 1979.

A further study of scale-effects was conducted by Bakhtar and Barton, 1984 using samples of the type illustrated in Figure 5d and Figure 18. These studies are incorporated in the next topic as they also gave insight into the need for a re-think about stress-transformation (from principle stresses σ_1 and σ_2 onto an inclined plane, in the form of the geotechnically important shear stress (τ) and normal stress (σ_n).

5 STRESS TRANSFORMATION, JRC (mobilized) AND SHEAR STIFFNESS

An important subject that goes beyond the more common distinction that we make between constant normal stress and 'constant' normal stiffness shear testing of rock joints (the latter actually not constant in reality), is the correct transformation of stress. The subject of concern is the transformation of stress from a principal (2D) stress state of σ_1 and σ_2 to an inclined joint, fault or failure plane, to derive the commonly required *shear and normal stress components* τ *and* σ_n. If the surface onto which stress is to be transformed does not dilate, which might be the case with a fault at residual strength, or for a thickly clay-filled discontinuity, *then* the assumption of co-axial or co-planar stress and strain is no doubt *more* valid.

If on the other hand dilation is involved (as in Figure 14), then stress and strain are no longer co-axial. In fact the plane onto which stress is to be transferred should be an *imaginary plane* since continuity is assumed. Non-planar rock joints, and failure planes through dense sand, or through over-consolidated clay, or through compacted rockfill, are neither imaginary *nor are they non-dilatant* in nature. This

problem nearly caused a rock mechanics related injury, when Bakhtar and Barton, 1984 were attempting to biaxially shear a series of ten 1 m^3 samples, applying shear and normal stress to the 130 cm long diagonal fractures (which were without weathering effects).

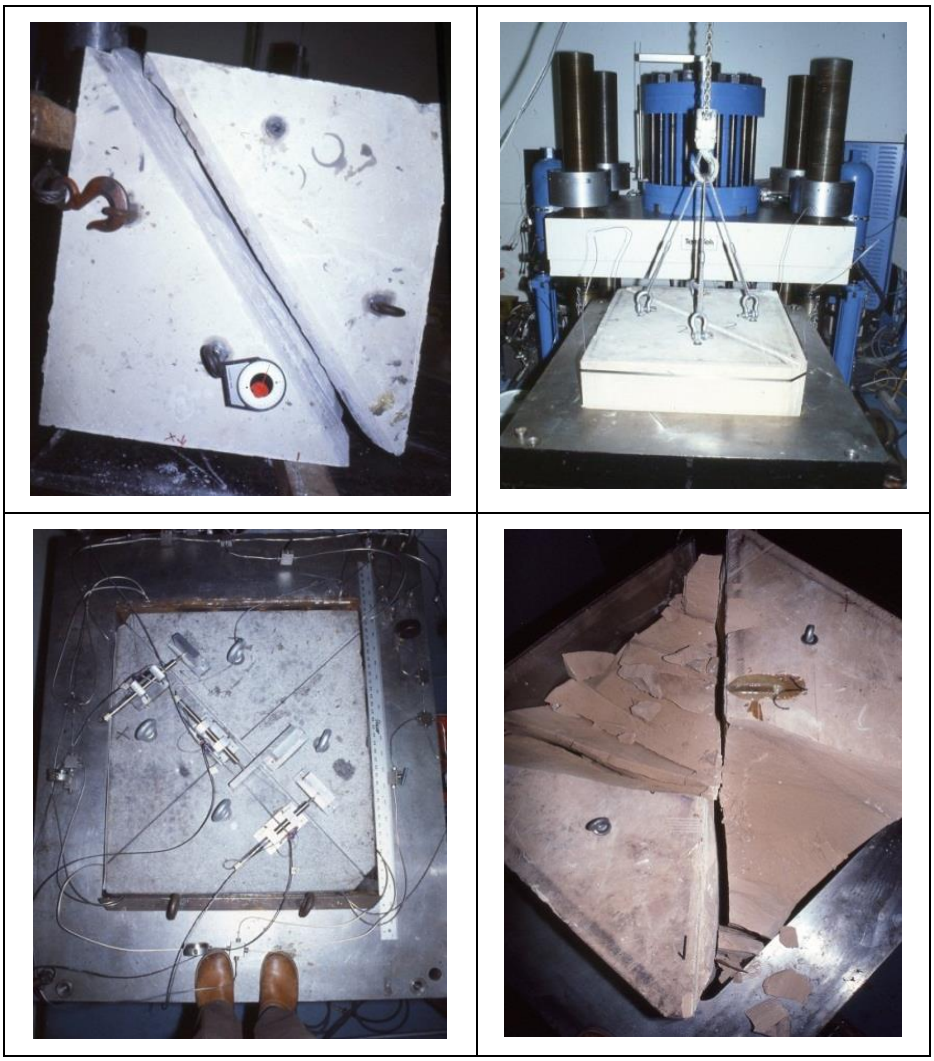

Figure 18. Sample loading test set-up and tilt testing of 1 m^3 samples of rock, hydrostone and concrete by TerraTek colleague Khosrow Bakhtar in the early 1980's (in a pre-Schlumberger era). Note the tilt testing (at 1 m^3 scale), lowering a lightly clamped sample into a test frame, LVDT instrumentation, and a (rare) sheared sample of an undulating fracture in sandstone. Bakhtar and Barton, 1984.

The experimental set-up and a tilt test are shown in Figure 18. The sample preparation was unusual because of principal stress (σ_1) controlled-speed-tension-fracturing: (see triangular flat-jacks in top-left photo). This allowed fractures to be formed in a controlled manner, with less roughness than typical for (laboratory-formed) tension fractures. Figures 19 and 20 show the stress application and related stress transformation assumptions, presented in three stages.

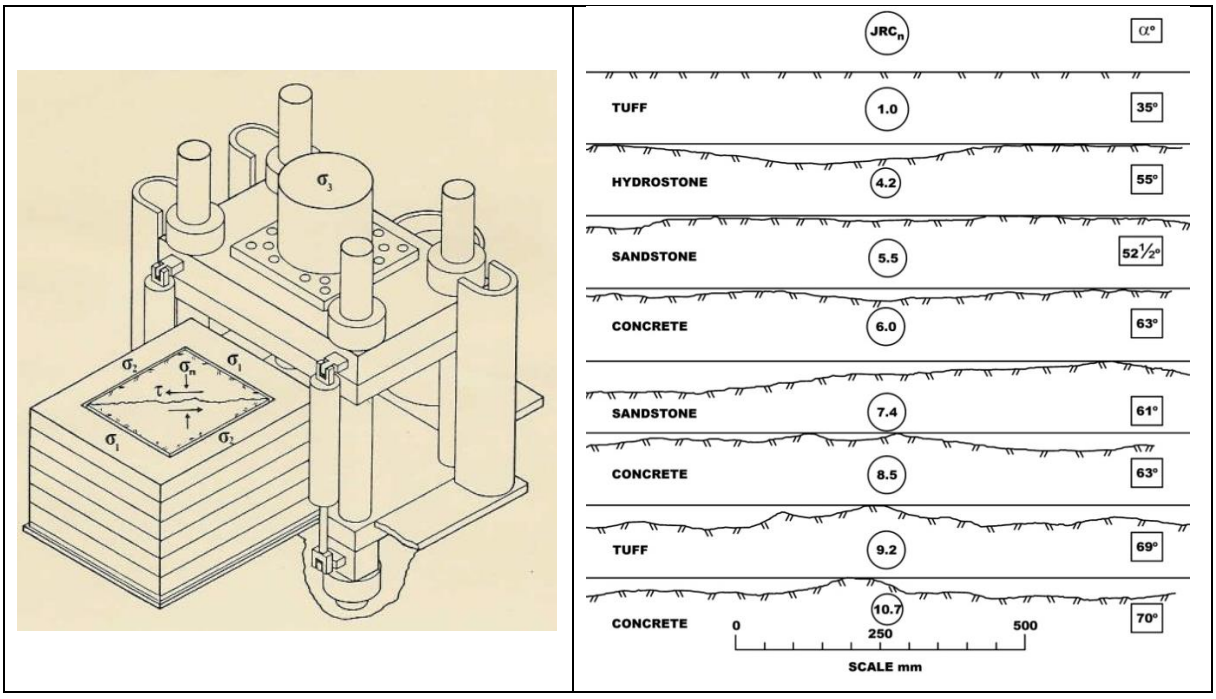

Figure 19 The TerraTek 1m³ 'cube-machine' biaxial (or poly-axial) loading facility. (This facility is now owned by Schlumberger). The roughness profiles were obtained by the simple techniques shown in Figure 5d. The JRC_n values were obtained by back-analising the large-scale (1300mm long) tilt tests which were performed on the 1 m³ diagonally-fractured samples. Bakhtar and Barton, 1984

The rock mechanics near-injury occurred when a (σ_1-applying) flat-jack burst at 28 MPa, damaging pictures on the laboratory walls and nearly injuring the writer who was approaching to see what the problem was. The sample illustrated in Figure 18 (with the photographer's shoes, pre-test stage) was transformed into ejected slabs, and ejected high-pressure oil, as a result of the explosive flat-jack burst. These 1.3m long tension fractures gave tilt angles varying from 52° to 70°, and large-scale (L_n = 1.3 m) joint roughness coefficients (JRC_n) varying from 4.2 to 10.7. A clear scale effect was exhibited in relation to the 100mm long JRC_0 profiles shown in Figure 4.

The conventional stress transformation equations 6 and 7, and the dilation-corrected equations 8 and 9 are given below. It will be noted that a mobilized dilation angle is needed. A dimensionless model for mobilization of roughness (JRC_{mob}) is used, and is seen to have wider application in the BB modelling.

$$\left.\begin{aligned} \sigma_n &= \frac{1}{2}(\sigma_1+\sigma_2)-\frac{1}{2}(\sigma_1-\sigma_2)\cos(2\beta) \\ \tau &= \frac{1}{2}(\sigma_1-\sigma_2)\sin(2\beta) \end{aligned}\right\} \qquad \text{(6) and (7)}$$

$$\left.\begin{aligned} \sigma_n &= \frac{1}{2}(\sigma_1+\sigma_2)-\frac{1}{2}(\sigma_1-\sigma_2)\cos[2(\beta+d_{n\,mob})] \\ \tau &= \frac{1}{2}(\sigma_1-\sigma_2)\sin[2(\beta+d_{n\,mob})] \end{aligned}\right\} \qquad \text{(8) and (9)}$$

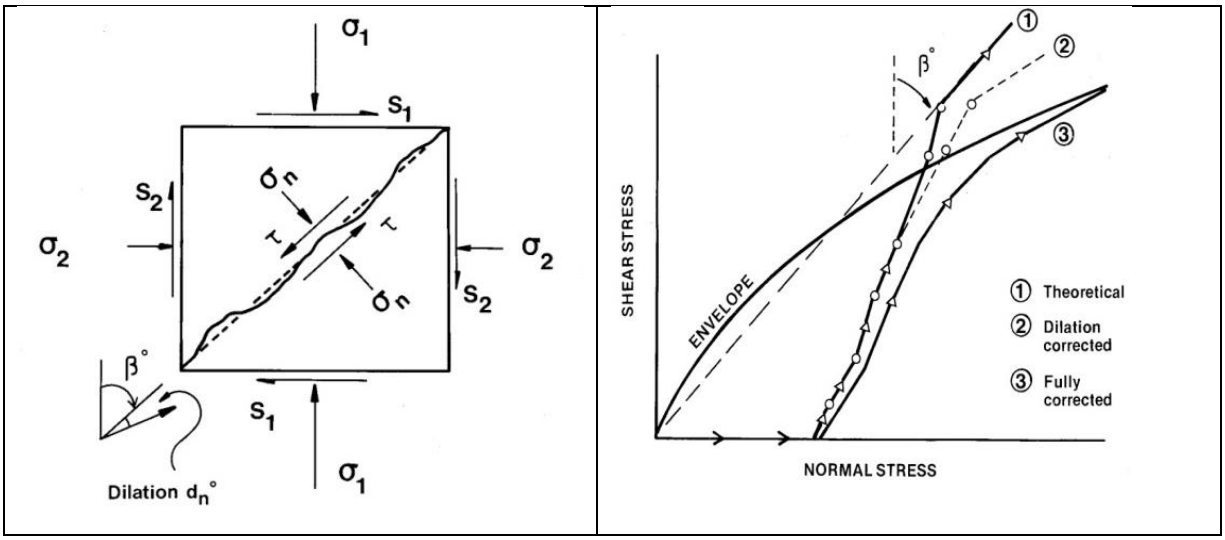

Figure 20 The assumed stress transformation components. In order to minimize boundary friction, molybdenum-greased double-teflon sheets (virtually fluid boundaries) and pairs of stainless-steel, 0 to 30 MPa flatjacks were used on all four sides of the 1 m³ blocks. it was assumed at first that failure was 'long overdue' when apparently reaching the location #1 in the right-hand diagram. In fact we were only just approaching the strength envelope, at location #3, so shear failure could not yet have occurred. Bakhtar and Barton, 1984.

Angle β is the acute angle between the principal stress σ_1 and the joint or failure plane. The peak dilation angle and mobilized dilation angle can be written as:

$$d_n^0(\text{peak}) = \frac{1}{2} JRC(\text{peak}) \log(JCS / \sigma_n') \qquad (10)$$

An estimate of the mobilized dilation angle $d_{n\,(mob)}$) for adding to the joint angle β, is as follows:

$$d_n^0(\text{mob}) = \frac{1}{2} JRC(\text{mob}) \log(JCS / \sigma_n') \qquad (11)$$

$JRC_{(mob)}$ is an important component of the Barton-Bandis joint behavior criterion. It is shown in Figure 21. It was developed by Barton, 1982 while analyzing the results of TerraTek's ONWI-funded 8m³ *in situ* heated HTM (hydro-thermo-mechanical) block test, which was performed by colleagues Hardin et al. 1982, at the Colorado School of Mines experimental mine.

The $JRC_{(mob)}$ concept illustrated in Figure 21 has the effect of 'compressing' a series of shear-displacement curves obtained from DST at widely different normal stresses (e.g. see Panel #1.2 in Figure 2) into a narrow band of behavior. Conversely, from the single JRC_{mob} /JRC_{peak} versus displacement δ/ δ_{peak} curve shown in Figure 21 we can generate (by hand if necessary) shear stress-displacement (and dilation-displacement) curves for widely different input data (JRC, JCS, ϕ_r) and widely different boundary (stress) conditions.

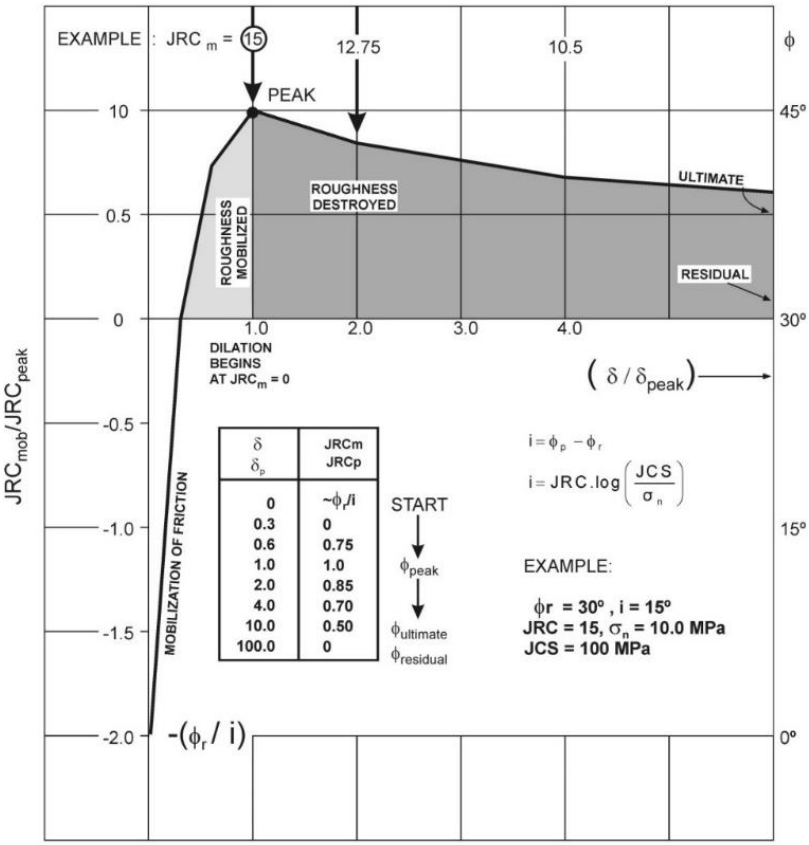

Figure 21 The dimensionless JRC $_{(mob)}$ concept was designed to match the details of joint or fracture behavior during direct shear testing. An example of this is shown in Figure 22. Note the different level of information compared to one 'peak' friction coefficient μ (top point of figure only) as used in petroleum geomechanics. Barton, 1982.

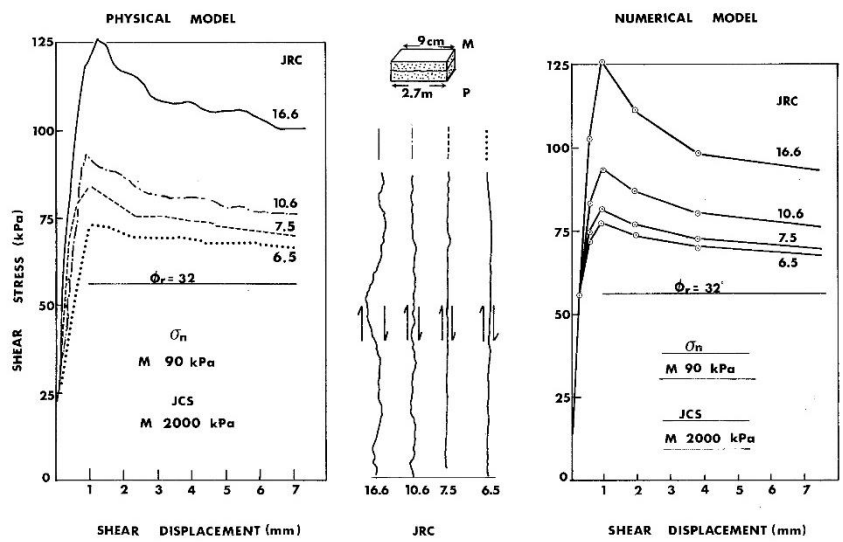

Figure 22 Generation of shear stress-displacement curves for four types of rock joint, as DST tested by Bandis, 1980. The 'numerical model' was generated by hand using the JRC$_{(mob)}$ concept, Figure 21. Barton, 1982.

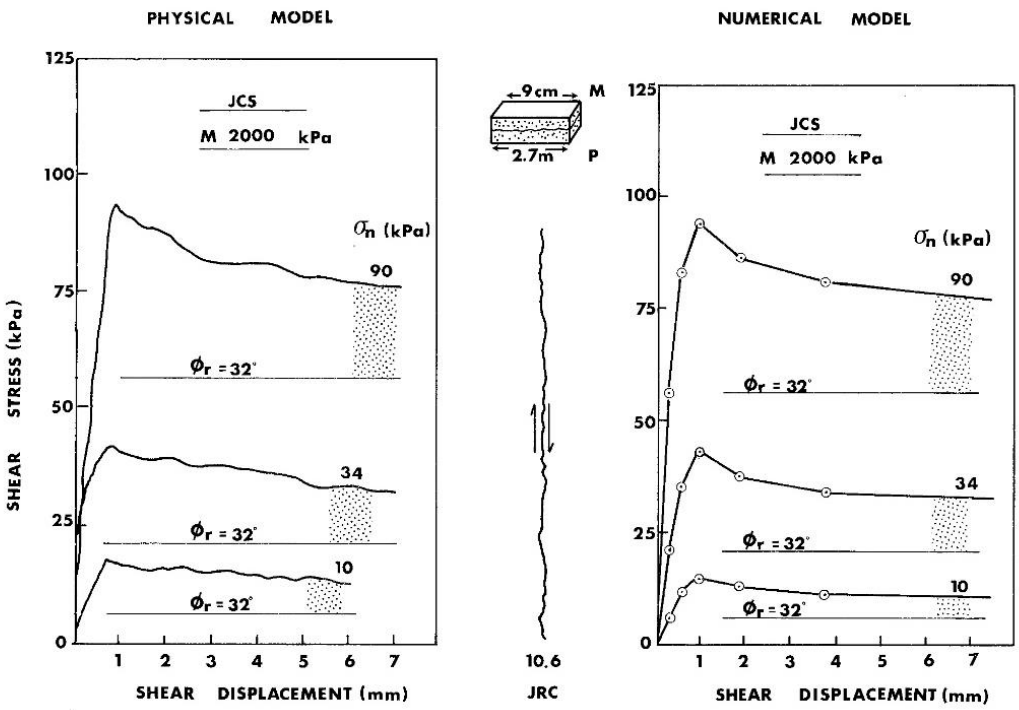

Figure 23 Generation of shear stress-displacement curves for one type of rock joint, as DST tested by Bandis, 1980 at three different levels of normal stress. The 'numerical model' was generated by hand.

Figures 22 and 23 demonstrate how the $JRC_{(mob)}$ concept is used to generate stress-displacement (and also dilation displacement) diagrams, for joints of any roughness, or any normal stress level. These were readily generated by hand (Barton, 1982) i.e. demonstrating the simplicity of the concept, devoid of 'black-box' software needs, as common in today's commercial software.

Since we now have a simple method of generating shear stress-displacement (and dilation-displacement) curves, we can take the method one stage further and generate shear stress-displacement (and dilation-displacement) curves for rock joints (or jointed blocks of rock) at various scales, using the JRC and JCS scaling equations (4 and 5) listed earlier, below Figure 14. In fact in the next section, considering joint apertures and joint conductivity, we will also be able to see how shearing and dilation affect the conductivity. We are then close to seeing the coupled nature of the Barton-Bandis model, which can be used for modelling rock mass deformation (i.e caused by tunnelling) and the joint-related flows (in 2D) towards the same tunnel.

We may experience that the set of joints suffering (slight) shearing and dilation may not be the same set that conducts most flow to the tunnel. It all depends on the magnitudes of JRC, JCS, ϕ_r and on the magnitudes of the initial hydraulic apertures prior to deformation. In the BB model we convert the dilation-induced aperture (E + ΔE) into the less altered e +Δe hydraulic aperture, using JRC_0 or $JRC_{(mob)}$ depending on whether opening / closing or shear/goudge production is occurring. This is described later in this chapter.

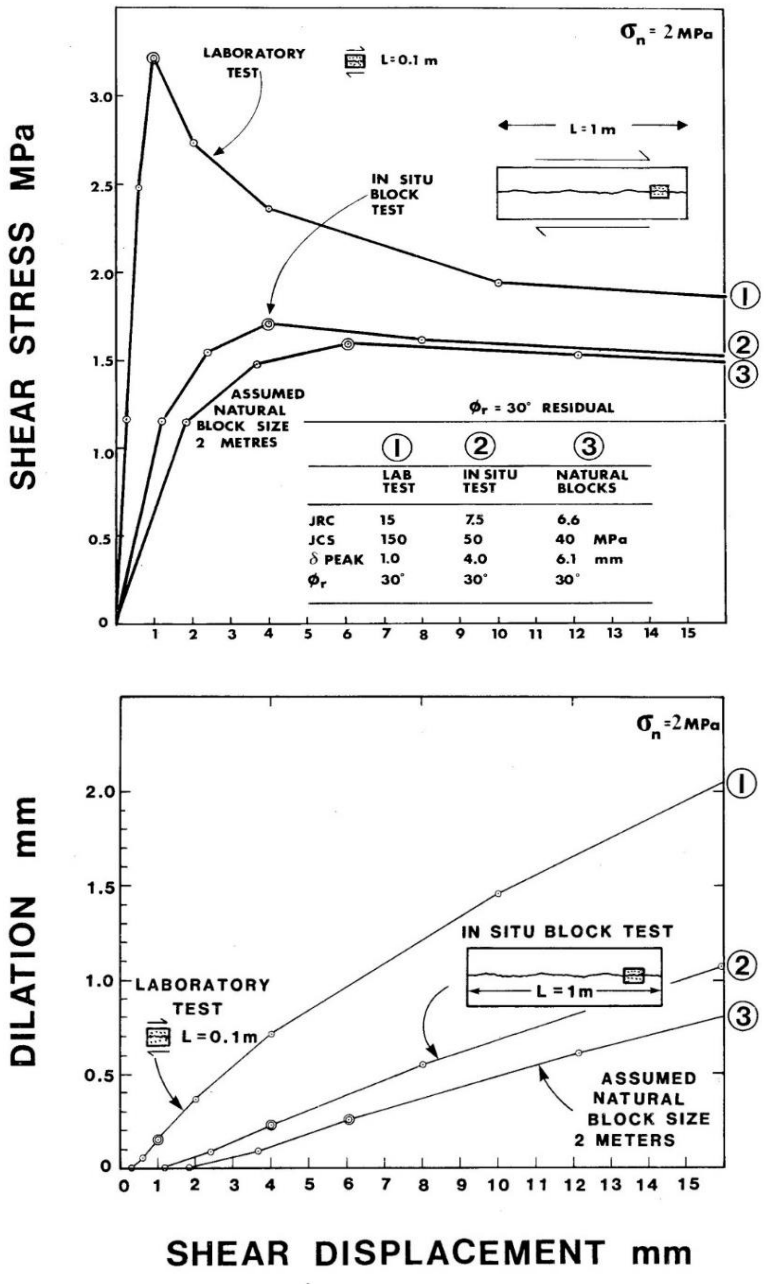

Figure 24 Generating shear-displacement-dilation behaviour, for three different block sizes. Barton, 1982. Note the inset showing the scaling assumptions from Bandis et al. 1981 equations 4 and 5. It will immediately be noted that, as experienced in practice, there is an increase in δ_{peak} as block size increases. Since there is also a reduction in peak shear strength, the peak shear stiffness Ks suffers a double scale-effect, and is lower than the values most numerical modellers are familiar with. This is shown later.

When estimating the values of JRC_n of most relevance to the given joint sets forming the rock mass (example block-sizes of 1m and 2m are shown in Figure 24) it is helpful to utilize the a/L method, which was sketched at small scale in Panels 4.1 and 4.2 of Figure 2. In Figure 25 this simple guide to scale effects is shown at a scale which could be used in practice. The black circles show imaginary a/L data that might

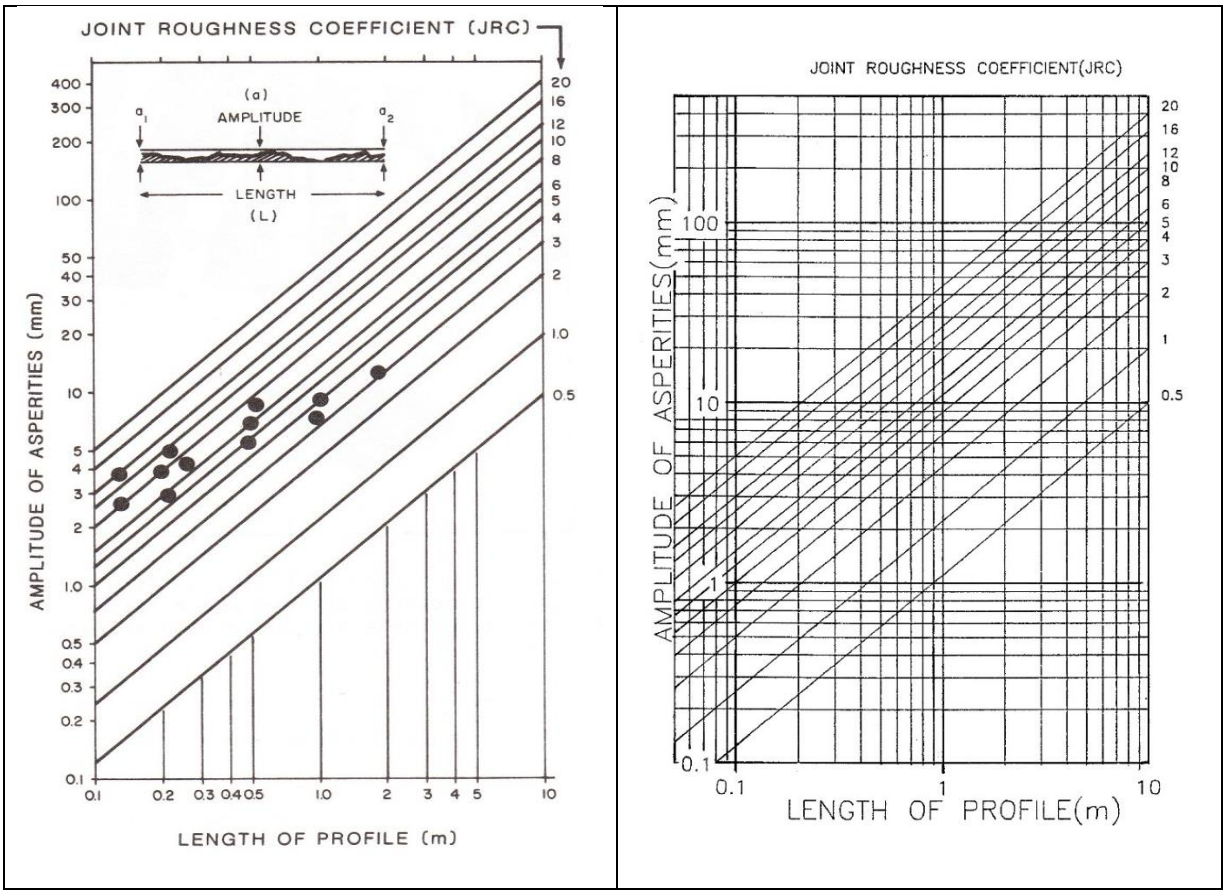

Figure 25 An illustration of the a/L method for estimating the large-scale JRC_n value. Note that at L = 10 cm scale $JRC_0 \approx 400$ a/L, while at L = 1m scale, $JRC_n \approx 450$ a/L. A field-logging sheet is given on the right, with interpolation down to 5cm scale for use when core-logging and needing to estimate JRC_0 . Barton, 1981.

have been collected by measuring convenient exposures of the joint set in question. In the case illustrated there is most data at L = 0.2m and at L = 0.5 m scales. There is only one data point for the imaginary mean block size of 2m. Nevertheless we must make the conservative extrapolation and use an estimate of JRC_n = 3 in this case, and check from equation 4 if this is consistent with the small scale (L = 15 to 20 cm) JRC_0 estimates of approx. 5 to 10 seen down to the left-hand side of Figure 25. The final value will be a question of engineering judgement, and may also include a look at the 130cm long profiles in Figure 19.

As noted in the figure caption of Figure 24, and in the inset to this same figure, an estimate of δ_{peak} is required in order to derive appropriate shear stress-displacement (and dilation-displacement) curves. A collection of some 600 DST results for block sizes from 10 cm to more than 3m assembled in Barton, 1982 indicated a rather wide spread of data for δ_{peak}. The statistics suggested the following formula as a workable approximation:

$$\delta_{peak} \approx L/500\ (JRC/L)^{0.33} \qquad (12)$$

where δ_{peak} is in meters and L is the block-size in meters.

Examples:

Lab. sample: L_0 = 0.1m, JRC_0 = 15. Equation 12 gives δ_{peak} = 0.0011m or 1.1mm.

In situ block: L_n = 1.0m, JRC_n = 7.5. Equation 12 gives δ_{peak} = 0.0039m or 3.9mm

As summarised in the figure caption to Figure 24, the double strength *and* δ_{peak} scale effect have a quite dramatic effect on the shear stiffness Ks. Many hundreds of DST data were assembled in Barton, 1982 and gave the trends shown in Figure 26 a. Data for clay-filled discontinuities, natural rock joints and model-material joint replicas are shown.

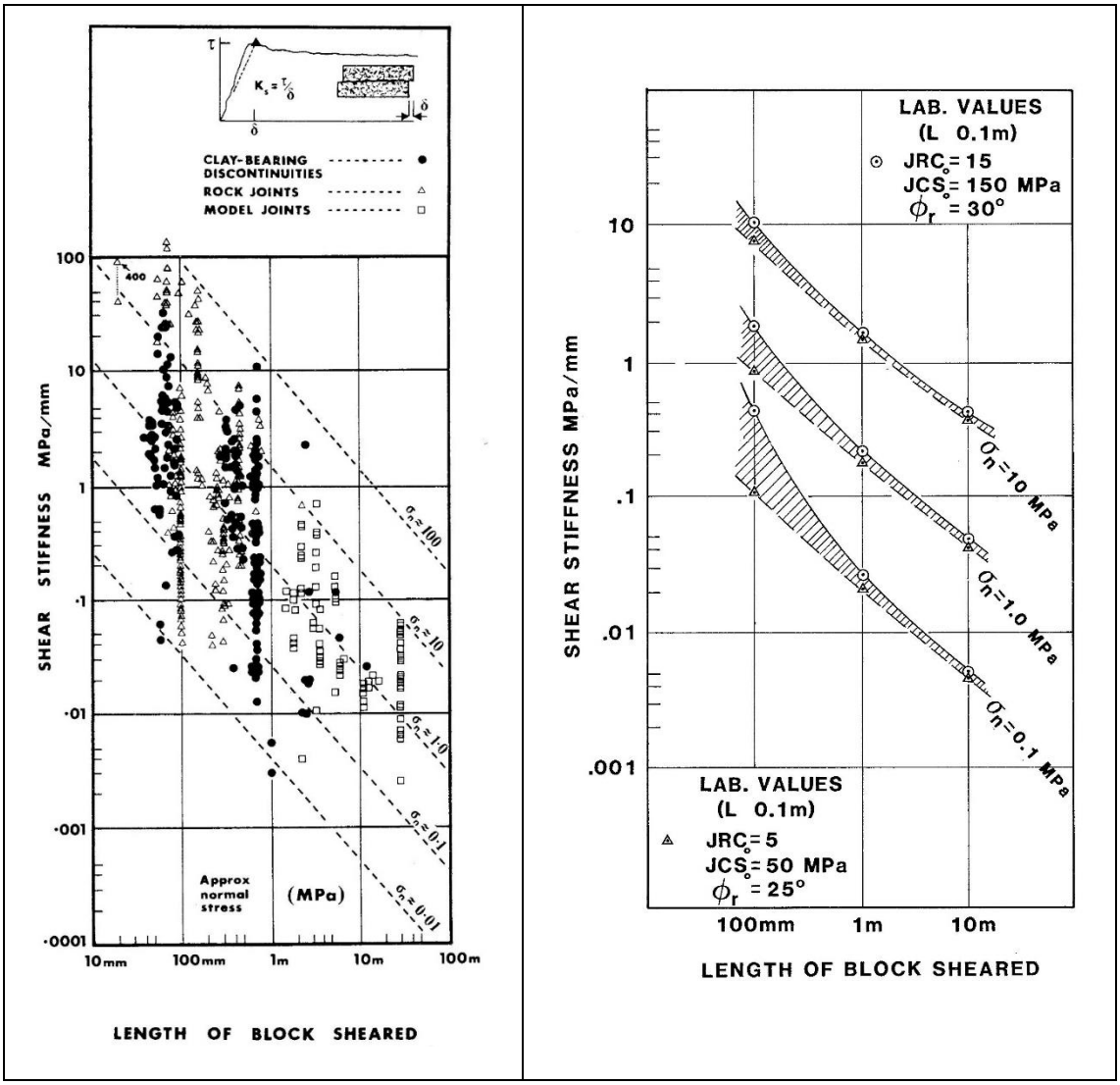

Figure 26 Left: Several hundred DST data for a variety of joints, filled-discontinuities and model-material replicas of joints. Note the strong scale effect, and also the approximate influence of the effective normal stress. Right: Predicted block-size scale and stress effects for a rough joint in hard rock, and for a smoother joint in weaker weathered rock. Care is needed when selecting Ks for modelling, as instruction manuals usually have the ratio Kn/Ks too small, even 1.0. (Kn = normal stiffness). This is incorrect. Barton, 1982.

In Figure 26, right-hand figure, a shear-stiffness prediction exercise is performed, using two widely different joint samples as a starting point. The top right-hand corner shows the parameters assumed for a very rough joint in hard unweathered rock (15, 150 MPa, 30°). The bottom left-hand shows the parameters assumed for a more planar weathered joint (5, 50 MPa, 25°). As we can see it is likely that shear stiffness Ks will often lie within the range of 0.1 to 1 MPa/mm for typical in situ rock block sizes and moderate (civil engineering) stress levels. In a later section of this chapter such low values will be contrasted with the much higher (x 50?) values of normal stiffness Kn, which of course emphasises the fundamental anisotropy of real rock masses, a property lost and forgotten in most continuum analyses, and even lost by some UDEC modellers.

6 THE CONDUCTIVITY OF ROCK JOINTS AND THE EFFECTS OF DEFORMATION

The theoretical Hagen-Poiseuille equation for the hydraulic conductivity (K) of a smooth parallel-plate, during laminar flow is:

$$K = (\rho g/\mu)\, e^2/12 = g e^2/12\nu \qquad (13)$$

where K is in units of velocity (LT^{-1}), g = gravity acceleration 981 cm/s/s (LT^{-2}), e = equivalent parallel plate aperture (L), ν = coefficient of kinematic viscosity of the fluid (ν= μ/γ = viscosity / density.

There are (at least) two types of joint aperture that need be considered when modelling the effect of joint deformation, namely the physical aperture (E) and the (theoretical) hydraulic aperture (e). A key issue is how to correlate the hydraulic apertures (e) to the generally larger physical apertures (E). The following empirical conversion formula was developed by Barton, 1982 and more widely published by Barton et al. 1985. It is for correlating E and e in relation to roughness (JRC). This formula applies to normal closure effects. Olsson and Barton, 2002 extended the modelling of E and e to the case of (potentially) gouge-producing shearing effects, in this case involving joint aperture conversion using $JRC_{(mob)}$. This is shown later, in Figure 28.

$$E = (e\, JRC^{2.5})^{1/2} \qquad (14)$$

Where e and E are in units of μm

The kinematic viscosity *v* of water is 0.01 at 20° C and ρ=1 gm/cm^3 . Checking units we see that ν= μ/γ = viscosity / density, with units $ML^{-1}\, T^{-1}/ML^{-3} = L^2/T$). It follows that:

$K = ge^2/12\nu = 8175\ e^2$ (cm/s) (15)

Substituting $e \approx E^2/JRC_0^{\ 2.5}$ yields the following formula for hydraulic conductivity:

$K \approx 8175\ [E^2/JRC_0^{2.5}]^{\ 2} \times 10^{-10}$ m/s (16)

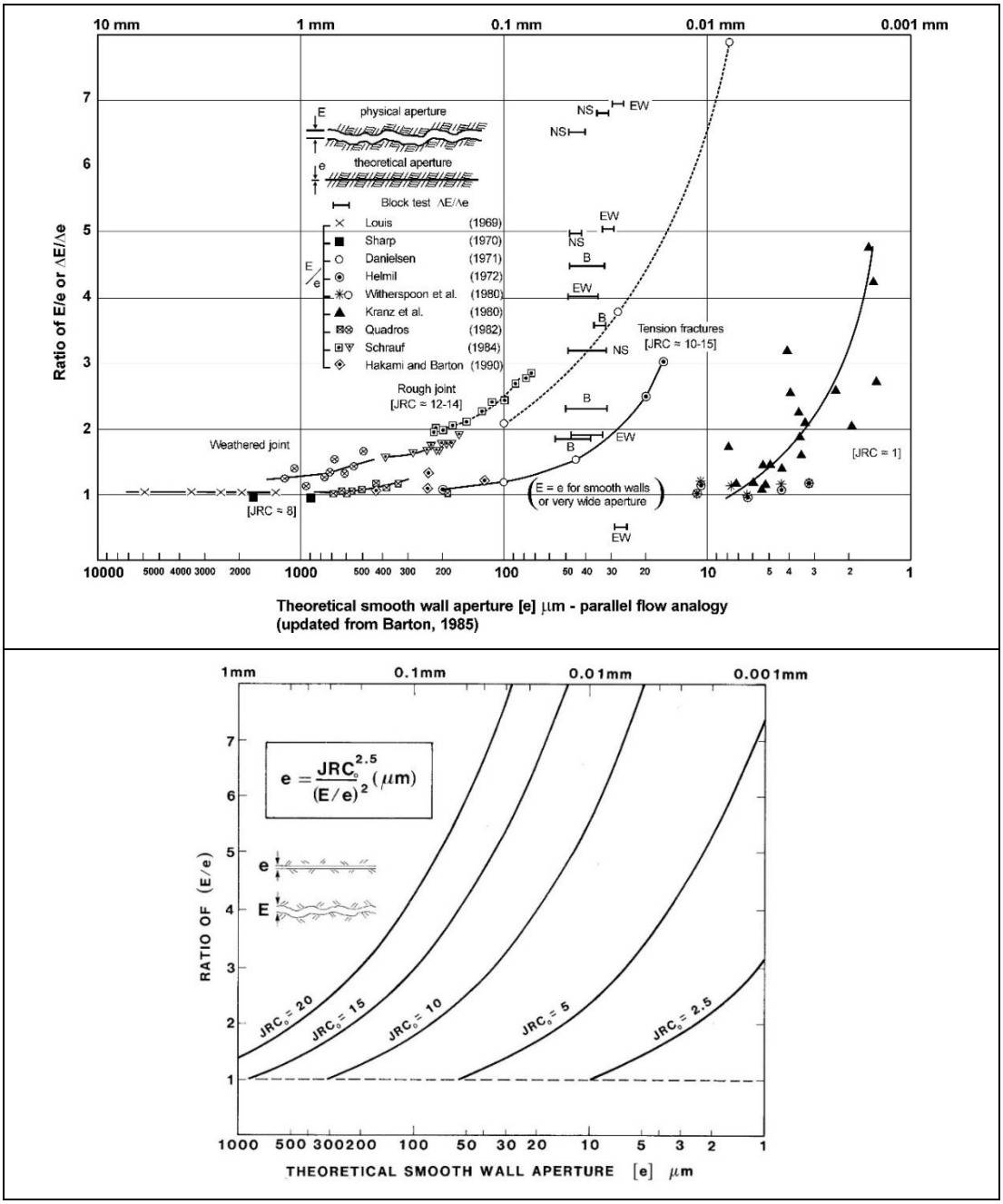

Figure 27 Top: Test data from which apertures e and E (or Δe and ΔE) were measured (Barton et al. 1985, updated by Quadros in Barton and Quadros, 1997. Bottom: The empirical model for converting between these two apertures was developed in Barton, 1982 and became a part of UDEC-BB in 1985.

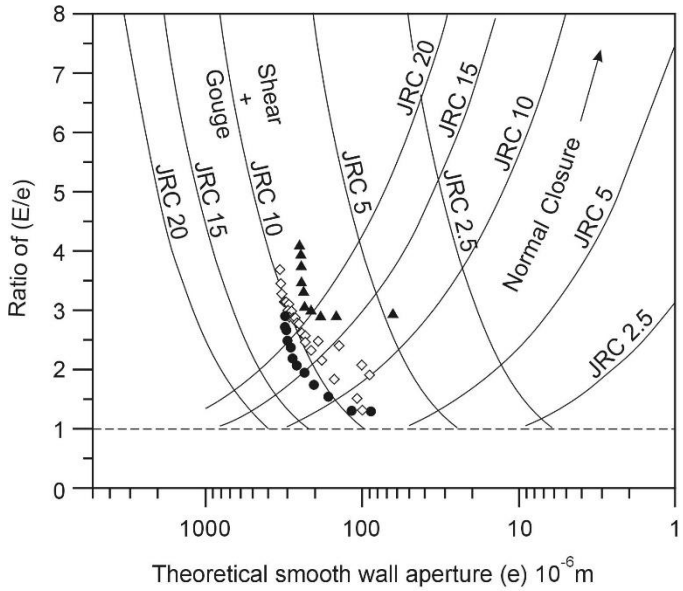

Normal Closure: $e = \frac{JRC_0^{2.5}}{(E/e)^2}$ } $e = E^2/JRC_0^{2.5}$

Shear+ Gouge: $e = \left(\frac{E}{e}\right) JRC^2$ } $e = \sqrt{E} \cdot JRC_{mob}$

Figure 28 Coupled shear-flow tests performed by Olsson, which were summarised in Olsson and Barton, 2002. In this figure the modification required to account for possible gouge-production during shear is shown in the 'left-hand' curves together with some data points for CSFT with samples having JRC_0 values of 7.2, 8.8, 9.7 and 12.2. The 'right-hand' curves are for closure/opening modelling, as in Figure 27. This figure shows equation 14 ('normal closure') while 'shear + gouge' involving $JRC_{(mob)}$ is equation 17.

Observations published by Makurat et al. 1990 indicated that CSFT (coupled shear flow tests) could cause gouge-production during shearing if stress levels were high in relation to JCS wall strengths. This could compromise both the physical (E) and hydraulic aperture (e) as interpreted from the 'cubic law'. Logically speaking there would be a whole range of stress/strength ratios (high strength, low stress) in which gouge or damage would be minimal. In those cases, the conversion involving the empirically derived roughness factor $JRC_0^{2.5}$ could be used in place of the Olsson and Barton equation with $JRC_{(mob)}$.

Examples showing the (BB-predicted) effect of shearing and dilation on the joint conductivity of joints of variable size, or on single samples tested at varied normal stress, are shown in Figure 29. Note that for simplicity a 'starting' aperture of e = 25 µm has been assumed in each case. As we shall see in the next section concerning normal stiffness, this assumption of an unchanged 25 µm is likely to be erroneous when changes of normal stress are being modelled. Of course in the UDEC-BB program, the 'starting' apertures are calculated more correctly from the following normal stiffness behaviour.

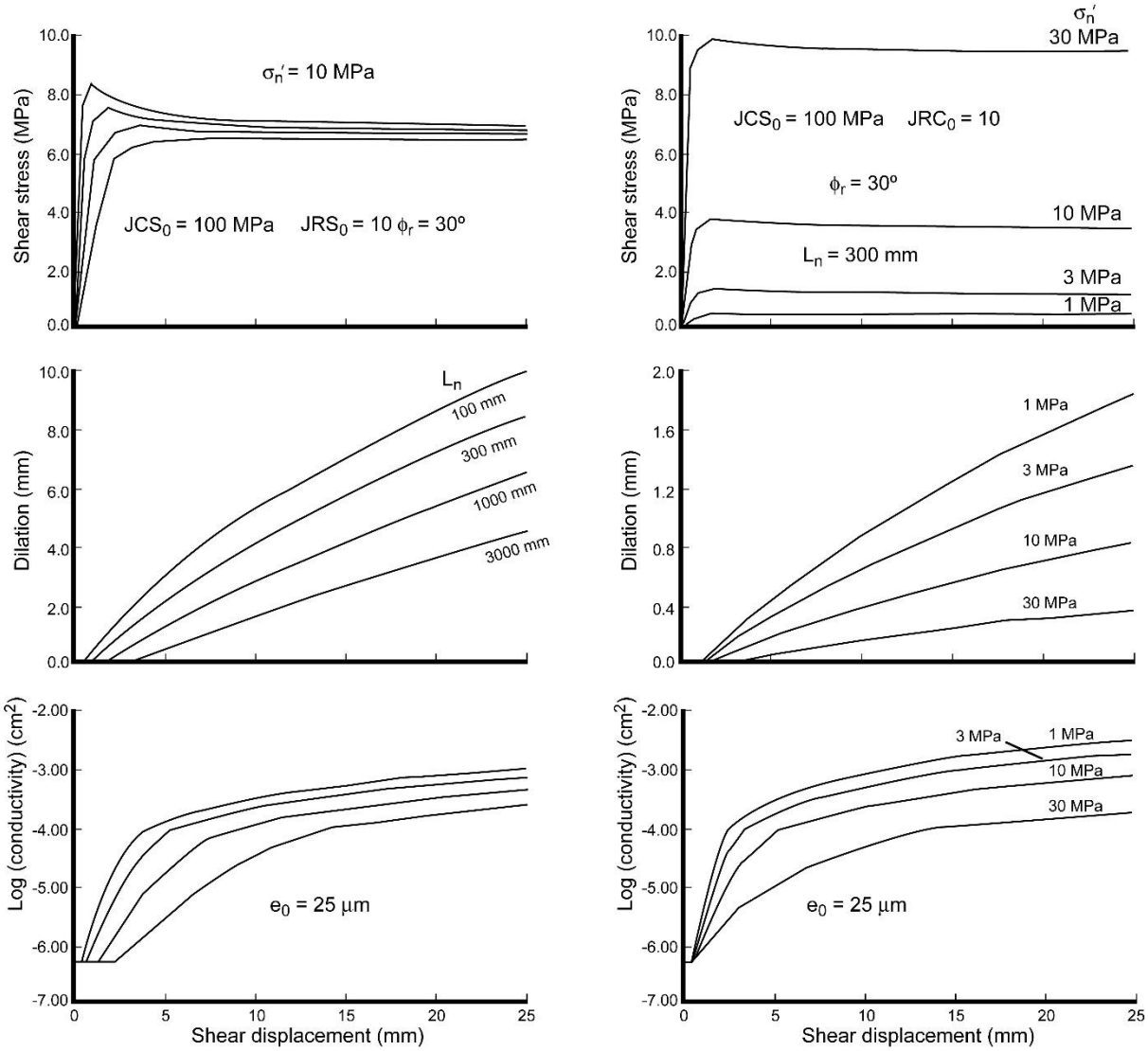

Figure 29 Examples of 'coupled' shear-dilation-conductivity modelling with the Barton-Bandis modelling assumptions. When block-size variations are involved (left) the delayed dilation and therefore delayed conductivity change can be noted. These curves were produced in 1983 by Bakhtar using a programmable HP calculator and the BB equations by now assembled in Barton, 1982. ONWI and AECL funded work were responsible for the 'finalization' of the BB model prior to its programming (by Mark Christiansson of Itasca) into the distinct element code UDEC-BB. Barton and Bakhtar, 1983, 1987.

Although unlikely to be noticed by petroleum geomechanics 'modellers' who are satisfied with linear friction coefficients and linear Mohr-Coulomb, these 'delay's may have influence on what should be the desired effect of massive hydraulic fracturing concerning the 'accompanying' microseismic evidence of shearing of natural fractures in the gas shales. This occurs at larger distances from the central elliptic regions of sand-propped fractures. (Barton, 2015).

As a result of seismic loading involving potential *reversals of shearing direction*, or as a result of some particular rock engineering excavation sequences which might result in a reversed shearing direction, one

needs to consider what is likely to happen to shear strength. In Figure 30, having due consideration of some reversed-shear DST appearing in the literature some decades ago, Barton, 1982 formulated the 'degrading of roughness' JRC related model shown in Figure 30. Progressing through some reversed cycles of shear would of course have the result of compromising some of the dilation-related permeability increases, and the 'gouge-production' adjustment shown in Figure 28 would obviously apply with successively renewed strength, due to accumulating damage and inevitable gouge-debris accumulations.

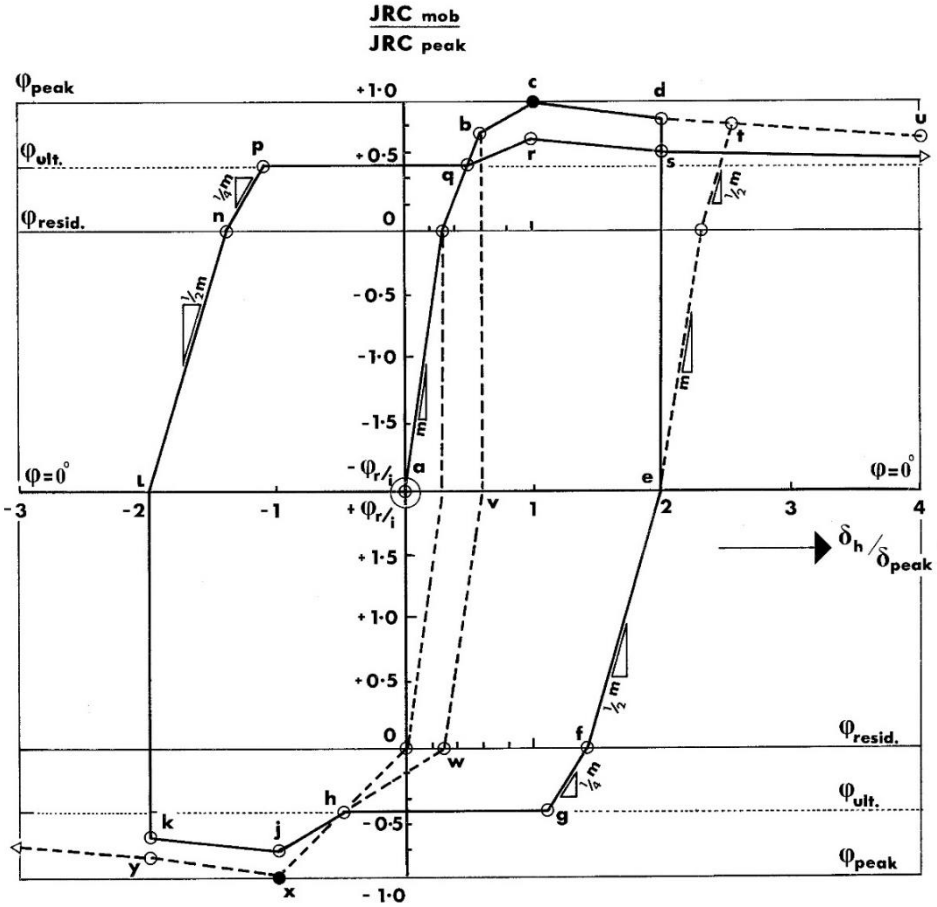

Figure 30 Reversed shear logic based on the dimensionless JRC$_{(mob)}$ concept. This model was developed in Barton, 1982 and shows gradual degradation of shear strength. A related model for the associated dilation has the shape of a 'saucer' which is thickening at its base by decreasing amounts with each cycle of reversal.

7 NORMAL CLOSURE OF JOINTS AND HOW TO MODEL IT

The diagrams and equations assembled in Figure 31 show how Bandis, 1980 formulated the normal closure behavior of rock joints, using the JRC and JCS parameters previously detailed in Barton and Choubey, 1977 and now easily acquired by performing the index tests shown in Figure 2. An important detail to note about normal closure behavior is that every sample tested has been unloaded and disturbed during the recovery period. This applies more to core than block samples, if the latter are 'banded' with steel belts prior to transport. This of course also applies to samples which will be tested in shear. However in this second case one is concerned about behavior of millimeter scale, while the closure of tight rock joints might be measured in a few tens of

microns. So near-removal of the effects of sample recovery by performing load-unload cycles becomes an important part of the testing procedure. The arbitrary but practical assumption is made that after about three to four load-unload cycles there is so little change that behavior can be considered as representative of undisturbed behavior.

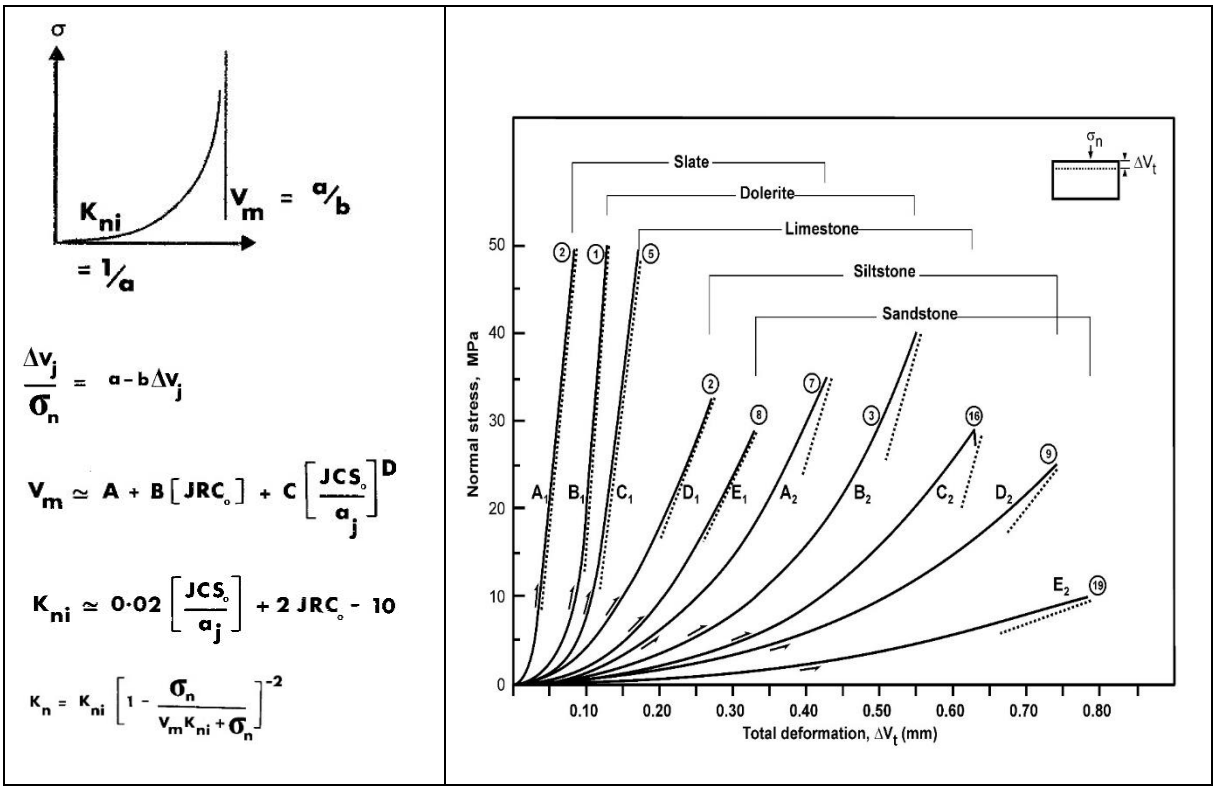

Figure 31 Left: The hyperbolic function (equation 18a) and related equations (equations 18 b, c, d) chosen by Bandis, 1980 to describe the highly non-linear behavior of closing interlocked rock joints. (This method and numerous experimental results were published in Bandis et al. 1983). The normal stiffness expression is a derivative of the hyperbolic function. Right: Experimental evidence acquired by Bandis show strong rock-type /rock joint-type dependence, but of course some of this can be explained by rock-type-characteristic values of JCS and JRC.

Figure 32 shows how normal stiffness behavior is interpreted as a net deformation of the joint, by subtracting the intact-rock deformation from the monitored behavior of load-unload cycles (sets of three are shown in Figure 33) from the 'rock-plus-joint' overall deformation. Wide differences in behavior from rock type to rock type and from joint type to joint type are indicated in Figure 33. A 'reservoir drawdown-and-injection' scenario is also demonstrated in Figure 33 (right-hand diagram).

8 CASCADING PROGRESSIVE FAILURE OF JOINTED ROCK MASSES

There is an almost 'universal' belief (for those not using the non-linear JRC/JCS model) that the shear

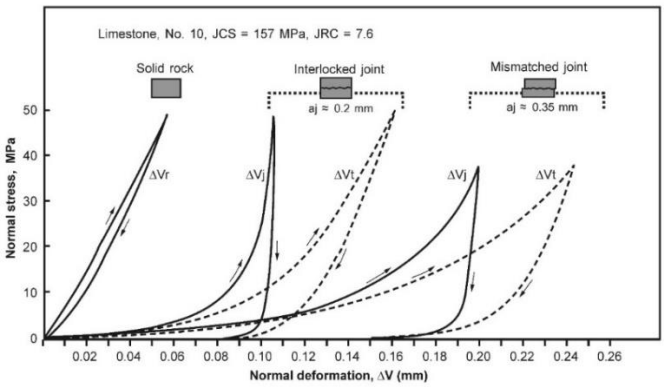

Figure 32 It is appropriate to 'define' normal loading behavior of rock joints by indicating the subtraction that has to be made of the elastic portion of the deformation associated with the intact matrix on either side of the joint. The net joint deformation is highly non-linear, but is made less so by shear deformation, or by mismatching (absence of inter-lock). Bandis et al. 1983.

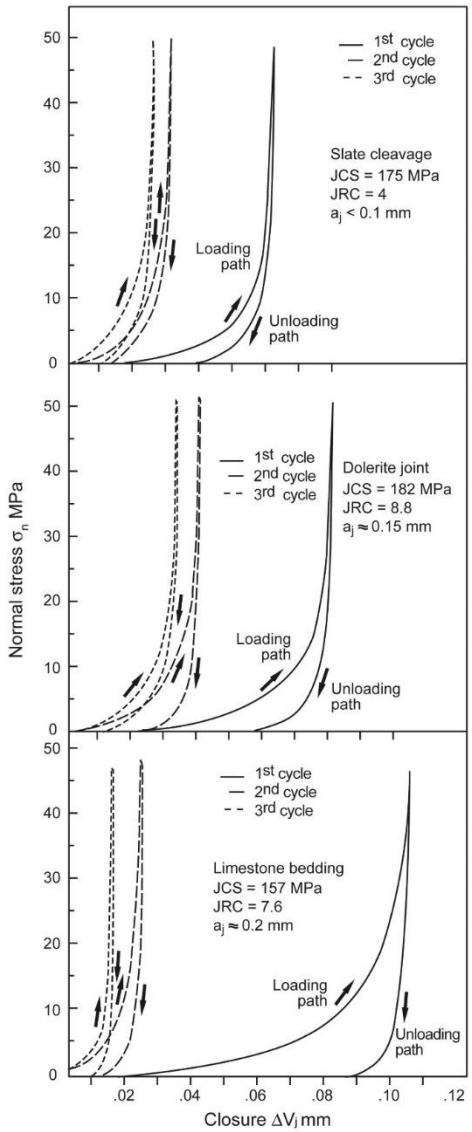

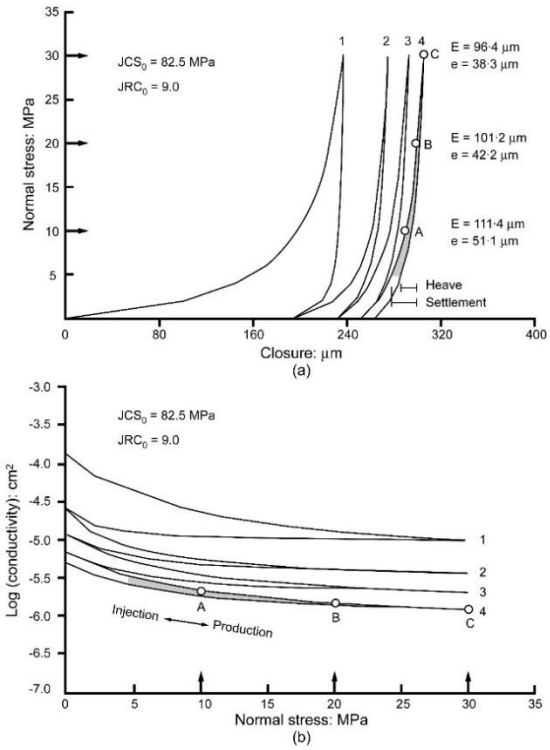

Figure 33 Left: Examples of normal stress-closure cycles for a cleavage joint in slate, for a rougher joint in dolerite, and bedding in hard limestone. Right: Using the BB-plotting routine programmed by Bakhtar on an HP calculator, to demonstrate the consolidating cycles seen on the left, and the assumed 'undisturbed behaviour' 4th cycle, onto which the modelled apertures e and E have been written at 10, 20 and 30 MPa. A 'reservoir drawdown and injection' effect have been shaded on the conductivity curves. Barton et al. 1985.

strength of rock joints consists of cohesion and friction, and that one can add c + σ_n tan ϕ. The assumed cohesive strength is actually a purely 'arithmetic' construction due to linearized strength envelopes, and represents something hypothetical in relation to the reality of increasing curvature (friction angle plus dilation angle increase) experienced close to zero normal stress. Barton, 1971 measured this lack of actual cohesion, even for the case of extremely rough tension fractures. The 'total friction' angle may reach 80° or more when normal stress is extremely low. The 'cohesion intercept' is an arithmetic convenience, but potentially exaggerates the shear strength actually available.

When on the other hand we consider the possible shear strength of *rock masses*, the same Mohr-Coulomb equation automatically comes to most people's minds. It is assumed that 'c' can again be added to 'σ_n tan ϕ'. In this case there may be a genuine cohesive strength component due to the 'necessary' failure of 'intact bridges', where joint sets do not 'line-up' as potential failure surfaces. However this time there is another type of problem. While the cohesion is no longer hypothetical but real, the problem is that it fails at much smaller strain than the mobilization of frictional strength along the newly formed fresh and rough fracture surfaces. These in turn may be stiffer than the lower strength (and possibly weathered) natural joints (i.e. those capable of shearing because of adverse orientations. There may aslo be clay-filled shear zones or faults, with their smaller-and-later response.

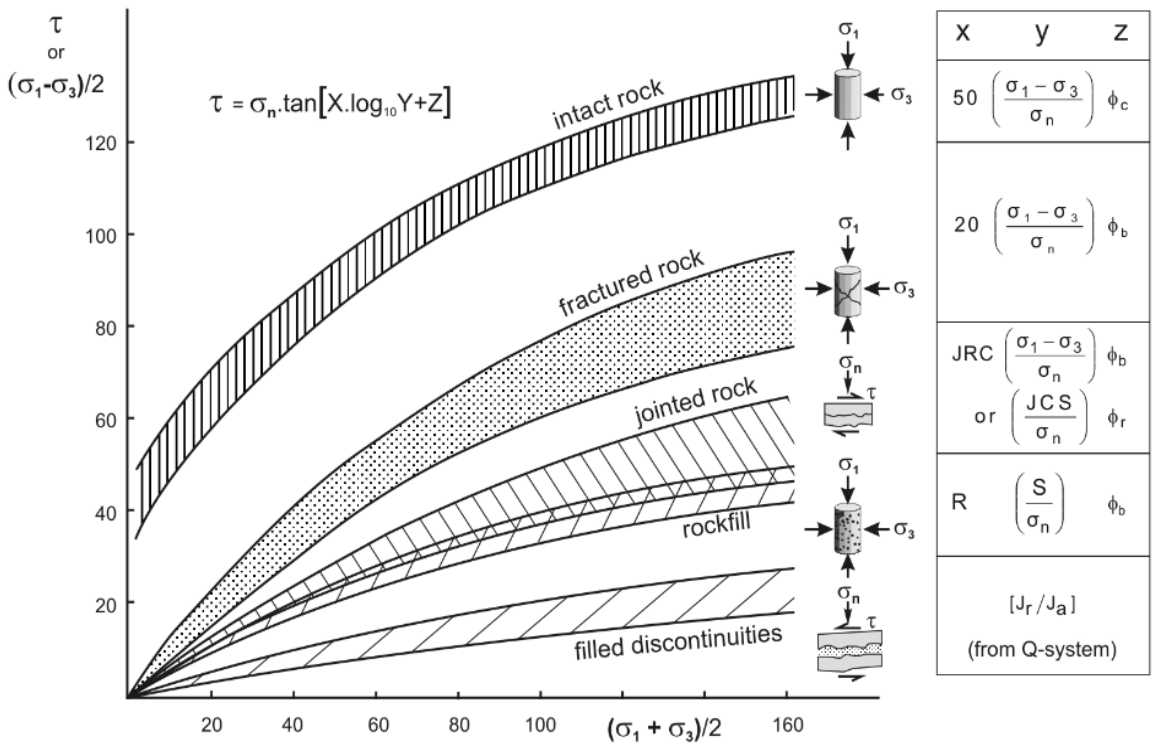

Figure 34 The components of the shear strength of rock masses, as assembled in Barton, 1999. When considering the shear strength of rock masses with possible intact portions of rock along the potential failure surface(s) it must be realized that these four components (excluding rockfill) are unlikely to

resist shear failure at the same shear strain. A 'cascading' progressive mobilization is involved from the upper to the lower curve at successively increasing shear strain (assuming filled discontinuities are also present).

A crude and non-conservative way to make allowance for the different components, and assume (when estimating by hand) that contributions can be added as if occurring at the same strain, but with the smallest-strain cohesion ignored, is illustrated in Table 1. With the aid of a computer one could mobilise the various components at their respective strains. How often do we see this done? Since the answer is clear we must conclude that it is time for change.

Table 1 A crude (and probably non-conservative) way to account for three of the components illustrated in Figure 33. Cohesion is ignored (this is conservative) but the three remaining fracture, joint, and filled-discontinuity components are imagined, for ease of hand calculation, to mobilize at the same strains.

FEATURE	Joint #1	Minor fault	Joint #3	Intact bridge (failed at small displacement (*)
Small-scale strengths JRCo JCSo Phi r	 14 75 29°	Jr = 1.5 Ja = 4 $\tau/\sigma_n = 1.5/4$	 12 55 28°	 18 150 32°
Large-scale strengths(est.) JRCn JCSn Phi r Block-size Ln (m) Large-scale undulation (?)	 9 45 29 2 to 4 m (+ i = 4°)	Jr = 1.5 Ja = 4 $\tau/\sigma_n = 1.5/4$ (+ i = 0°)	 6 30 28 3 to 5 m (+ i = 2°)	 12 90 32° 1m (+ i = 4°)
Partial safety factors	1.2	1.3	1.2	1.1
Final strength components	45°/1.2 = 37.5°	21°/1.3 = 16°	37°/1.2 = 31°	56°/1.1 = 51°

Length (m)	50	25	30	20

Weighted mean strength 34°	$\frac{37.5° \times 50 + 16° \times 25 + 31° \times 30 + 51° \times 20}{50 + 25 + 30 + 20}$

(*) Clearly it is extremely conservative to ignore an intact rock cohesion of e.g. 25 MPa

9 A BRIEF COMPARISON OF MOHR-COULOMB AND BARTON-BANDIS MODELLING

Rock masses may range from almost intact, through well jointed, to heavily crushed, due to increased proximity to fault zones. The result is variable geometrical patterns resulting from several types of joint sets with their variable roughness and continuity. Notwithstanding an implied need for engineering rationalization, the assessment of strength for such complex media as rock masses cannot be approached on the basis of a single generic strength criterion.

The type, frequency and orientation of the jointing and faulting define the likely modes of deformation, and some indication of the likely ultimate failure mechanism. In significant volumes of rock there may be two or three classes of discontinuities (natural and stress-induced fracturing) which can become involved in the pre-peak and post-peak deformation and failure. Rock mechanics practitioners to date have generally adopted one of the following two approaches for the characterization and engineering study of *jointed* rock.

- A *discontinuum* approach, in which the geologic structure is explicitly represented and in turn controls the modes of deformation and mechanisms of ultimate failure (prior to modelling of appropriate rock mass reinforcement).
- A *continuum* approach, which involves a semi-empirical simulation of the rock mass, transforming the *in situ* (actual) discontinuous state into a hypothetical continuous medium, in which the weakening and softeninginfluence of jointing is allowed for implicitly

Due to the complexity we must resort to numerical UDEC-BB or 3DEC simulations. A useful starting point, and a demonstration of the fundamental differences between M-C and B-B can be gained by performing simulations of large scale biaxial and triaxial tests. These give a useful insight into mechanisms at failure, and comparisons of shear strength estimates based on the above non-linear strength criteria, with linear M-C criteria are quite revealing. Of course predictions from "global" continuum strength criteria (an example would be GSI-based H-B Hoek-Brown) are quite different to both. Contrasting B-B and M-C behaviour for an equally jointed 'rock mass' sample are shown in Figure 34.

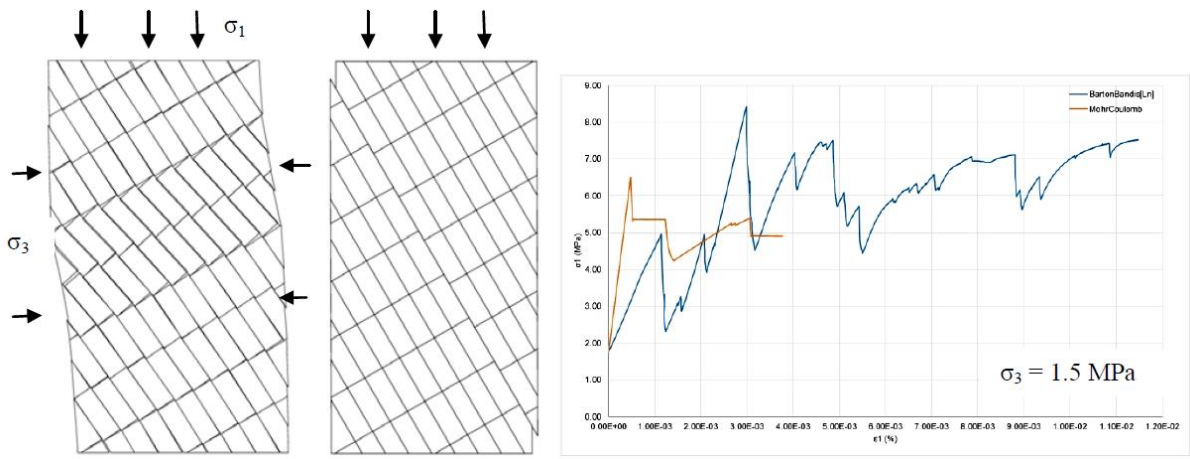

Figure 35 Contrasting stiffness and strength behaviour, assuming non-linear (BB – left block plot) and linear (MC – right block plot). Due to the non-linearity of BB simulations compared to the linear (or bi-linear 'ramping') in the case of MC, significant block rotations are seen with BB which tend to be absent with MC. A comprehensive set of comparisons with numerous geometric and boundary conditions are given by Barton and Bandis (2018, in preparation).

Such diverging approaches, coupled with the inherent complexity of jointed rock behaviour, have created unfortunate barriers that, to date, have prevented comprehensive and generally accepted

approaches to rock mechanics, as needed for solving rock engineering problems. Discontinuum and continuum mechanics approaches are applicable to specific rock mass conditions, and *cannot be used interchangeably*, as summarized below:

- The *continuum* (implicit) approach is appropriate where the frequency and orientation of jointing are such that no preferential paths of stress-strain responses are present. Such conditions are present in an estimated <10% of rock masses.
- The *discontinuum* (explicit) approach is appropriate when the geological structure controls anisotropy, deformation modes, and strength. Such conditions are applicable to the vast majority (> 90%) of rock masses.

10 CONCLUSIONS

1. The authors are aware of some 50 equations for evaluating JRC. While this should be considered gratifying, the great majority are rather complex descriptions of a topological nature, or linked to 3D laser profilometric analysis. The simple performance of tilt tests seems mostly to have escaped those analyzing roughness and 'improving' JRC.
2. This chapter addresses the recommended methods of describing and performing index tests of rock joints by means of the two basic parameters JRC and JCS suggested by Barton, 1973.
3. Due to the considerable further work of the two authors (including that with Choubey and Bakhtar) and subsequent correction for block-size scale effects, mostly from Bandis, the methods of predicting non-linear joint behavior (stiffness, strength, dilation, conductivity, each with deformation) have become known as the Barton-Bandis or BB model. We must thank Bandis for his unmatched contribution during too short a lifetime (1951-2016 †)
4. At the end of this chapter we have shown the fundamental differences between linear (Mohr-Coulomb, MC) and non-linear BB. The differences are worthy of attention.

11 REFERENCES

Bakhtar, K. and Barton, N. 1984. Large scale static and dynamic friction experiments. Proc. 25th US Rock Mechanics Symp. Northwestern Univ., Illinois.

Bandis, S. 1980. Experimental studies of scale effects on shear strength, and deformation of rock joints. Ph.D. Thesis, Univ. of Leeds, Dept. of Earth Sciences.

Bandis, S., Lumsden, A. & Barton, N. 1981. Experimental studies of scale effects on the shear behaviour of rock joints. Int. J. of Rock Mech. Min. Sci. and Geomech. Abstr. 18, 1-21.

Bandis, S., Lumsden, A.C. & Barton, N. 1983. Fundamentals of rock joint deformation. Int. J. Rock Mech. Min. Sci. and Geomech. Abstr. Vol. 20: 6: 249-268.

Barton, N. 1971. A relationship between joint roughness and joint shear strength. Proc. of Symp. of Int. Soc. Rock Mech. Rock Fracture, Nancy, paper I.8, 20 p.

Barton, N. 1973. Review of a new shear strength criterion for rock joints, Engineering Geology, Elsevier, Amsterdam, Vol. 7, pp. 287-332. Also NGI Publ. 105, 1974.

Barton, N. & Choubey, V. 1977. The shear strength of rock joints in theory and practice. Rock Mechanics 1/2:1-54. Vienna: Springer. Also NGI Publ. 119, 1978.

Barton, N. & Hansteen, H. 1979. Very large span openings at shallow depth: Deformation magnitudes from jointed models and F.E. analysis," 4th Rapid Excavation and Tunnelling Conference, RETC; Atlanta Georgia, Vol. 2: 1131-1353. Eds A.C. Maevis and W.A. Hustrulid. American Institute of Mining, Metallurgical, and Petroleum Engineers, Inc. New York, New York, 1979.

Barton, N. 1981. Shear strength investigations for surface mining. 3rd Int. Conf. on Stability in Surface Mining, Vancouver, Ch. 7: 171-192, AIME.

Barton, N. & Bandis, S. 1982. Effects of block size on the shear behaviour of jointed rock. Keynote Lecture, 23rd US Symposium on Rock Mechanics, Berkeley, California.

Barton, N. 1982. Modelling rock joint behaviour from in situ block tests: Implications for nuclear waste repository design. Office of Nuclear Waste Isolation, Columbus, OH, 96 p., ONWI-308, September 1982.

Barton, N., Bandis, S. & Bakhtar, K. 1985. Strength, deformation and conductivity coupling of rock joints. Int. J. Rock Mech. & Min. Sci. & Geomech. Abstr. 22: 3: 121-140.

Barton, N. & Bakhtar, K. 1987. Description and modelling of rock joints for the hydrothermalmechanical design of nuclear waste vaults. Atomic Energy of Canada Limited. TR-418. Volumes I and II. (Published following TerraTek, Salt Lake City contract work in 1983).

Barton, N. & Quadros, E.F. 1997. Joint aperture and roughness in the prediction of flow and groutability of rock masses. Proc. of NY Rocks '97. Linking Science to Rock Engineering. Ed. K. Kim, pp. 907-916. Int. J. Rock Mech. and Min. Sci. Vol. 34: No. 3-4.

Barton, N. and Bandis, S.C. 1990. Review of predictive capabilities of JRC-JCS model in engineering practice. International Symposium on Rock Joints. Loen 1990. Proceedings, pp. 603-610, 1990.

Barton, N. 1995. The influence of joint properties in modelling jointed rock masses. Keynote Lecture, *8th ISRM Congress*, Tokyo, 3: pp. 1023-1032, Balkema, Rotterdam.

Barton, N. 1999. General report concerning some 20th Century lessons and 21st Century challenges in applied rock mechanics, safety and control of the environment. Proc. of 9th ISRM Congress, Paris, 3: 1659-1679, Balkema, Netherlands.

Barton, N. 2014. Shear strength of rock, rock joints, and rock masses: problems and some solutions. Keynote lecture, Eurock, Vigo, 14p.

Barton, N. 2015. Where is the non-linear rock mechanics in the linear geomechanics of gas shales? Keynote lecture. China Shale Gas Conf., Wuhan.

Barton, N.R. 2016. Non-linear shear strength descriptions are still needed in petroleum geomechanics, despite 50 years of linearity. 50th US Rock Mech. Houston. ARMA 16, paper 252, 12 p.

Barton, N. and Bandis, S. 2017 (in preparation). *Engineering in jointed and faulted rock.* Taylor and Francis, est. 750p.

Makurat, A., Barton, N., Rad, N.S. & Bandis, S. 1990. Joint conductivity variation due to normal and shear deformation. Int. Symp. on Rock Joints. Loen 1990. Proceedings, pp. 535-540.

Olsson, R. & Barton, N. 2001. An improved model for hydro-mechanical coupling during shearing of rock joints. Int. J. Rock Mech. Min. Sci. & Geomech. Abstracts, 38: 317-329. Pergamon.

Patton, D.F. 1966. Multiple modes of shear failure in rock and related materials. *PhD Thesis*, University of Illinois, 282p.

Pratt, H.R., Swolfs, H.S., Brace, W.F., Black, A.D. & Handin, J.W. 1977. Elastic and transport properties of *in situ* jointed granite. *Int. J. Rock Mech. Min. Sci., 14*: 35–45. UK: Pergamon.

Cundall, P.A., Fairhurst, C. and Veogele, M. 1977. Computerized design of rock slopes using interactive graphics for the input and output of geometrical data. *Proc. of 16th U.S Symp. on Rock Mech., (1975), ASCE, New York.*

Zoback, M.D. 2007. *Reservoir Geomechanics*. Cambridge Univ. Press. 461p.